AD-A278 529

CUMENTATION PAGE

Form Approved
OMB No. 0704-0188

2. REPORT DATE	3. REPORT TYPE AND DATES COVERED
	ANNUAL 1 Sep 92 - 31 Aug 93

4. TITLE AND SUBTITLE

MAPPING CRUST AND UPPER MANTLE STRUCTURE BENEATH SOUTHERN EURASIA

5. FUNDING NUMBERS

F49620-92-J-0470
61102F
2309
AS

6. AUTHOR(S)

Dr Donald V. Helmberger

7. PERFORMING ORGANIZATION NAME(S) AND ADDRESS(ES)

Dept of Geological/Planetary
California Institute of Technology
Seismological Lab, 252-21
Pasadena, CA 91125

8. PERFORMING ORGANIZATION REPORT NUMBER

AFOSR-TR- 94 0202

9. SPONSORING/MONITORING AGENCY NAME(S) AND ADDRESS(ES)

AFOSR/NL
110 DUNCAN AVE SUITE B115
BOLLING AFB DC 20332-0001

Dr Stanley K. Dickinson

10. SPONSORING/MONITORING AGENCY REPORT NUMBER

11. SUPPLEMENTARY NOTES

12a. DISTRIBUTION/AVAILABILITY STATEMENT

Approved for public release;
distribution unlimited

12b. DISTRIBUTION CODE

13. ABSTRACT *(Maximum 200 words)*

In this study of lateral variations in compressional velocity in the uppermost mantle underneath the Tibetan plateau, 353 Pn travel times were collected for 44 Tibetan earthquakes at 46 seismic stations. The inverse method and procedures in this study differ from previous Pn tomography studies in that corrections were applied to the biases caused by (1) event mislocation by ISC, (2) mantle velocity gradient, and (3) large-scale variations in crustal thicknesses. Main results to date are: (1) the average P velocity value for the uppermost mantle in Tibet is 7.93±0.17 km/s; (2) the average P velocity gradient in the upper 150 km of the mantle is 3.1×10^{-3} 1/s; (3) the 2D P velocity image of the region includes a low velocity zone in the north central Tibet, and two high velocity zones in the western and eastern flanks of Tibet; and (4) in much of the area inside Tibet, the crustal thickness exceeds 70 km. Another important finding of this study is that event relocation (see the bias 1) plays a very important role in reliably retrieving the detailed lateral variations in 2D P velocity image. Corrections to biases 2 and 3, seem to have a greater effect on the average of the velocity image, causing over-estimations.

14. SUBJECT TERMS

15. NUMBER OF PAGES

16. PRICE CODE

17. SECURITY CLASSIFICATION OF REPORT	18. SECURITY CLASSIFICATION OF THIS PAGE	19. SECURITY CLASSIFICATION OF ABSTRACT	20. LIMITATION OF ABSTRACT
(U)	(U)	(U)	(U)

Annual Technical Report

1 September 1992 - 31 August 1993

Name of Contractor:	California Institute of Technology
Effective Date of Contract:	1 September 1992
Contract Expiration Date:	31 August 1994
Contract Number:	F49620-92-J-0470
Principal Investigator:	Donald V. Helmberger (818)395-6998
Program Manager:	Dr. Stanley K. Dickinson
Short Title of Work:	Mapping Crust and Upper Mantle Structure Beneath Southern Eurasia

Sponsored by
AFOSR/NL
110 Duncan Avenue, Suite B115
Bolling AFB DC 20332-0001
Contract #F49620-92-J-0470

Seismological Laboratory
Division of Geological and Planetary Sciences
California Institute of Technology
Pasadena, California 91125

Table of Contents

Summary

A back-projection algorithm is applied to 353 P_n travel time measurements to image the lateral variations in compressional velocity in the upper most mantle in and around Tibet. Since large-scale lateral variations are known to exist in the Tibetan crustal structure, we refined the apparent P_n slowness measurements prior to the tomographic inversion. These refinements are based on a recently developed relocation procedure (Zhao & Helmberger, 1991), and on a new theoretical understanding of head wave propagation in 3D media with velocity gradients (Zhao, 1993). These refinements are crucial in obtaining a high-quality velocity image.

We obtained an average P-velocity value for the uppermost mantle of 7.93 km/s, and an average mantle P-velocity gradient of 3.1 X 10^{-3} s^{-1} for Tibet. The final 2D P-velocity image in the uppermost mantle is characterized by a large (7 to 9 degrees in dimension) low-velocity (down to about 7.78 km/s) region in north central Tibet, and by large high-velocity (up to 8.11 km/s) regions in the western and eastern flanks of Tibet.

By attributing the remaining slowness residuals to systematic variations in crustal thickness among 28 source/receiver regions, we estimated the crustal thicknesses in those regions. The result is characterized by large thicknesses (>70 km) inside the Tibetan plateau, and by decreases in the crustal thickness toward the southern, eastern and western boundaries of the plateau; the thicknesses at and beyond these boundaries are similar to those in the rest of Eurasia. The rate of the decreases appear to be higher toward the western boundary.

Rigorous analyses of resolution and error suggest that

(i) there is a pronounced difference between the tomographic velocity image obtained with and without the refinements to the P_n slowness measurements, indicating a significant improvement in the quality of our inversion by these refinements;
(ii) random errors in measuring earthquake origin times and locations, and in the P_n arrival times, should not cause errors of more than 0.1 km/s in the velocity image;
(iii) the resolution is generally within 6 to 10 degrees.

We have also compared the images in P_n velocity and in crustal thickness obtained in this study with those localized results from numerous pervious studies in and around Tibet. General agreement has been found between ours and most previous results. The few exceptional disagreements can be interpreted largely as the result of effects of a complex medium, such as the effects of mantle velocity gradient, which have not been carefully accounted for in previous studies.

The velocity image obtained in this study is consistent with previous S-P{ travel time studies and geothermal/petrological studies, and is consistent with a mantle convection model in which a convective upwelling is occurring in north central Tibet and downwellings occurring in the surrounding regions (Molnar, 1988, 1990).

Lateral Variations in Compressional Velocities Beneath the Tibetan Plateau from P_n Travel-Time Tomography

Lian-She Zhao[1] and Jiakang Xie[2]
[1]Seismological Laboratory 252-21
California Institute of Technology
Pasadena, CA. 91125
[2]Department of Earth and Atmospheric Sciences
Saint Louis University
3507 Laclede Avenue
St. Louis, MO 63103

INTRODUCTION

The Tibetan Plateau, the Himalaya and the Karakoram are the most spectacular consequences of the collision of the Indian subcontinent with the rest of Eurasia in Cenozoic time (Fig. 1). Accordingly, the deep structure beneath them provides constraints on both the tectonic history of the region and on the dynamic processes that created these structures (Molnar, 1988).

There have been numerous studies of seismic velocity structure beneath Tibet. Studies of surface waves (eg. Bourjot & Romanowicz, 1992), P_{nl} waveforms (Holt & Wallace, 1990), and S-P differential travel times (Molnar & Chen, 1984; Pettersen & Doornbos, 1987; Molnar, 1990) have indicated that there are significant lateral variations in seismic velocities in and around Tibet. There seemed to be a tendency for velocities to be lower in north central Tibet (Molnar, 1990). This tendency, while inferred from very sparse data coverage, has been intriguing because of its suggestion of a probable convective upwelling in north central Tibet and downwellings in the surrounding regions (Molnar, 1988, 1990), which are in agreement with the observations of Cenozoic volcanism in north central Tibet (Burke et al., 1974; Deng, 1978; Kidd, 1975; Sengor & Kidd, 1979;

Molnar et al., 1987).

Previous tomographic inversions of P_n travel times have been conducted in the western U.S. (eg., Hearn et al., 1991). The P wave velocity images from these inversions generally correlate well with the major tectonic features in those areas. In P_n tomography, it is desirable to invert for the lateral variations of P wave velocity in the uppermost mantle. When there is a velocity gradient in the upper mantle, however, P_n observed at different distances samples mantle P-wave velocities through different depth-ranges. This has been shown to be the case in Tibet (Song et al., 1985; Holt & Wallace, 1990). Previous P_n tomography studies have ignored the effect of the mantle velocity gradient. In an area where this gradient exists, images of lateral variations in P wave velocity may be contaminated by vertical variations in the mantle P wave velocity. Recently Zhao (1993) developed mathematical formulations which enable us to calculate head wave travel times in the presence of lateral structural variations, and to estimate and correct for the upper mantle velocity gradient, if this gradient is nearly constant with the varying depth.

In this study, we apply the mathematical formulations of Zhao (1993), as well as the relocation procedure by Zhao & Helmberger (1991) to 44 seismic events and 353 P_n travel times to obtain P wave slownesses along paths confined to the uppermost mantle. These slownesses are then input to a tomographic back-projection algorithm to obtain a laterally varying, 2D P wave velocity image in the uppermost mantle beneath the Tibetan Plateau. Under a further assumption that the remnant slowness residual, which is not diminished by tomography, is caused primarily by the vertical travel time delays at the sources and stations, we also invert for the crustal thicknesses for 28 sub-regions in Tibet. We also conduct rigorous analysis of error and resolution of the P wave velocity inversion, and test the sensitivity of the 2D P velocity image to (i) event relocation, (ii) the

corrections of effects of large-scale lateral structural variations, and (iii) the corrections of effects of mantle velocity gradient. We will demonstrate that (i) plays a key role in correctly resolving the detailed lateral variations in the 2D P-velocity image, whereas (ii) and (iii) mainly affect the average (DC level) of the P velocity image. Finally, the 2D P velocity image and the crustal thicknesses will be compared to the numerous localized studies conducted *prior* to this study, and will be discussed in terms of tectonic processes underneath the Tibetan Plateau.

DATA

We collected 353 P_n arrival times from 44 earthquakes (Table 1) which occurred inside Tibet. Fig. 2 shows the ray coverage. The distance range of the data is 3-15 degrees. P_n arrivals at greater distances were not used, since, from synthetics using model TIP, which was developed for Tibet by Zhao et al. (1991), deep turning P waves arrive before P_n beyond 18 degrees. Of these travel times, we repicked 42 to judge the reliability of the ISC (International Seismological Centre) picks. Generally, they agree within 0.5 seconds. We rejected the P_n arrival times yielding apparent P_n velocities less than 7 km/s or greater than 9 km/s.

The parameters of the events used in this study are obtained by the relocation procedure of Zhao & Helmberger (1991). These parameters are listed in Table 1. The number of the P_n phase picks from the event is also listed in Table 1, under "N". In Table 2, we listed the stations used in this study, with vertical travel time delays (b'_j). The latter are calculated from the available regionalized models, including the models of Holt & Wallace (1990), Zhao et al. (1991), and Zhao & Helmberger (1993). More details of the relevant calculation will be discussed later.

INVERSE METHODS

Computerized tomography has previously been applied to P_n travel times to image the P velocity in the upper mantle (eg., Hearn et al., 1991). In general, t_{ij}, the P_n travel time from an ith source to a jth station can be expressed by

$$t_{ij} = V_{ij}^{-1} X_{ij} + a_i + b_j \quad , \tag{1}$$

where X_{ij} is the source to receiver horizontal distance, V_{ij} is the apparent P wave velocity, a_i and b_j are vertical travel time delays at the source and receiver, respectively (Hearn et al., 1991). Zhao (1993) has shown that this relation is valid for the head waves traveling in complex waveguides, except that a_i and b_j should be calculated using local structures.

Method to estimate a_i, b_j and mantle velocity gradient

In previous studies, a_i and b_j are solved for iteratively. For this study, *a priori* knowledge of the averaged velocity structures within and outside Tibet is available (Holt & Wallace, 1990; Zhao et al., 1991; Zhao & Helmberger, 1993). Our approach is therefore to use this *a priori* knowledge to estimate a_i and b_j approximately, and subtract these approximate estimates from the travel times before the tomographic inversion. a_i and b_j estimates thus obtained do not include the effects of smaller-scale lateral variations in crustal thickness, since we do not have *a priori* knowledge of these variations.

Another difference between our method and previous inverse methods is that in the current inversion, we take into account the P velocity gradient in the upper mantle, which is known to exist beneath the Tibetan Plateau (Song et al., 1985; Holt & Wallace, 1990). An important effect of the mantle velocity gradient is that the P_n phase observed at different distances samples P velocities in different depth-ranges, and the resulting P velocity image from tomography will be

somewhat contaminated by the depth variations of P velocity in the mantle.

Numerically, both the approximate corrections for a_i and b_j and the corrections for mantle gradient are possible only with the new formulations recently developed by Zhao (1993). These formulations related the P_n travel times to the P velocities in the uppermost mantle in the presence of both lateral structural variations and a constant velocity gradient in the upper mantle. To use these formulations, we rewrite equation (1) as

$$\frac{1}{V_{ij}} = \frac{t_{ij}-a_i-b_j}{X_{ij}} \quad . \tag{2}$$

Denoting the estimates of a_i and b_j by a'_i and b'_j, respectively, we have

$$\frac{1}{V_{ij}} \approx \frac{1}{V'_{ij}} = \frac{t_{ij}-a'_i-b'_j}{X_{ij}} \quad . \tag{3}$$

When a constant velocity gradient is present, the mantle P-velocity distribution can be expressed as

$$V(z) = V(z_0)(1+c(z-z_0)) \quad , \tag{4}$$

where $V(z)$ is the depth-varying P velocity, z_0 is the depth of Moho, and c is a constant whose product with $V(z_0)$ gives the mantle velocity gradient for a flat Earth. For a spherical Earth, the velocity gradient is $(c - 1.6\times10^{-4})V(z_0)$ when the units for c and $V(z_0)$ are km^{-1} and km/s, respectively (*cf.*, Helmberger, 1973). Zhao (1993) shows that when such a constant velocity gradient exists, V_{ij} in equations (1) and (2) can be expressed as

$$V_{ij} = V_{ij}^0\left(1 + c^2X'^2_{ij}/24\right) \quad , \tag{5}$$

where V_{ij}^0 is the P velocity in the uppermost mantle averaged along the (i,j) th path, and X'_{ij} is the horizontal distance that a ray *travels in the mantle.* Now we introduce a small residual

$$\epsilon_{ij} = \left(V_{ij}^0 - \overline{V}(z_0)\right)\left(1 + c^2 X'^3_{ij}/24\right)$$

$$\approx V_{ij}^0 - \overline{V}(z_0) \qquad (6)$$

where $\overline{V}(z_0)$ is V_{ij}^0 averaged over all of the (i,j) pairs. Substituting equation (6) into (5) leads to

$$V_{ij} = \overline{V}(z_0) \qquad (7)$$

In practice we must use V'_{ij} (equation (3)) instead of V_{ij} when equation (7) is used; ϵ_{ij} will in that case contain, in addition to the right-hand side of equation (6), contributions from non-zero δa_i and δb_j, defined as

$$\delta a_i = a'_i - a_i \qquad (8)$$

and

$$\delta b_j = b'_j - b_j \quad . \qquad (9)$$

For an area where a number of different V'_{ij} are collected, $\overline{V}(z_0)$ and c can be solved by linear regression using equation (7).

Method used to obtain 2D P velocities in the uppermost mantle

Once $\overline{V}(z_0)$ and c are solved, V_{ij}^0 can be estimated for each of the (i,j) pairs using equations (3) and (5). Dividing the area under study into cells, we have from the definition of V_{ij}^0

$$\frac{1}{V_{ij}^0} = \frac{1}{X'_{ij}} \sum_k \Delta_{ijk} s_k + Res_{ij} \quad , \qquad (10)$$

where Δ_{ijk} is the line segment over which the (i,j)th path overlaps the kth cell, s_k is the slowness in the kth cell, Res_{ij} is the slowness residual, which is caused by errors in event origin times/locations, in the travel time readings, and in a'_i and b'_j, which are approximations of a_i and b_j and are used to calculate V_{ij}^{-1}

(equation (3)). Strictly speaking, deviations of the real uppermost mantle form a gridded, smoothly varying surface will also contribute to ϵ_{ij}; effects of this kind are known as the "modelisation error" (eg., Tarantola, 1987). Equation (10) forms a standard linear inverse problem for unknown s_k. We use a variation of the back-projection, or SIRT algorithm (eg., Humphreys & Clayton, 1988), described in detail by Xie & Mitchell (1990) to solve for s_k. In particular, we use the 9-point smoothing operation (Suetsugu & Nakanishi, 1985; Xie & Mitchell, 1990) between the iterations. This operation is used to overcome insufficient spatial data coverage, at a slight cost of resolution.

Method to estimate crustal thicknesses

In the back-projection calculation, s_k values are updated during the iterations to reduce the misfit between the inverse of V_{ij}^0 and $\frac{1}{X^t_{ij}}\sum_k \Delta_{ijk} s_k$. When the misfit stops decreasing, we end up with the final slowness model (final values of s_k) and some non-diminished Res_{ij} values. To the first order approximation we assume that Res_{ij} values are dominately caused by a'_i and b'_j, the imprecise estimates on a_i and b_j *prior* to the back-projection inversion, we then have

$$Res_{ij} \approx \frac{\delta a_i + \delta b_j}{X_{ij}} \quad . \tag{11}$$

At the time we obtain Res_{ij}, a_i and b_j are known, and a_i and b_j (therefore δa_i and δb_j) are not. Non-zero δa_i and δb_j values primarily result from the lack of smaller-scale variations in the crustal structure used to calculate a'_i and b'_j *prior* to the inversion. With the known Res_{ij} values, we can solve for δa_i and δb_j to obtain a_i and b_j values, which can then be used to infer the smaller scale crustal thicknesses (this is just a calculation inverse to one with which we obtained a'_i and b'_j). To make the inversion for δa_i and δb_j overdetermined, and to reduce

the probable effects of errors in origin times (Table 1), in event locations (Zhao & Helmberger, 1991) and in P_n arrival time readings (which also contribute to Res_{ij}), we merge the unknowns δa_i and δb_j into a new set of unknowns. To do so we divide the area under study into sub-regions with the following properties: (1) each of the lth sub-region contains either a group of sources or a group of stations, called a "sub-region of sources" or a "sub-region of receivers"; (2) within each sub-region, all of the a'_i and b'_j calculated for locations inside it have been constant, and (3) the geographic extent of each of the lth sub-region is small, so that the crustal thickness can be assumed constant. We now assume that δa_i and δb_j are constants within a given sub-region, *ie.*,

$$\delta a_i = \tau_l \tag{12}$$

for all of the ith sources located within the lth sub-region of sources, or

$$\delta b_j = \tau_l \tag{13}$$

for all of the jth station located within the lth sub-region of stations. $\tau_{l'}$ thus introduced form a new set of variables which is smaller in size than the unknowns δa_i and δb_j, provided that the number of sub-regions is small. Using Res_{ij}, we can now solve for τ_l in an overdetermined least-squares problem.

AVERAGE P_n VELOCITY AND MANTLE VELOCITY GRADIENT

The a'_i values are obtained with a laterally homogeneous velocity model (model TIP of Zhao et al., 1991). Values of b'_j are calculated from the models of Holt & Wallace (1990) and of Zhao et al. (1991). a'_i and b'_j are all estimated using the method of Zhao (1993). The resulting b'_j values are listed in Table 2.

The a'_i and b'_j values thus obtained are then subtracted from t_{ij} values to obtain apparent P_n velocity values, which were subsequently multiplied by a factor of $(R_E - D)/R_E$ to correct for a first-order effect of the earth's sphericity,

where R_E (=6371 km) and D (=55 km) are defined as the average radius of the earth and the average crustal thicknesses in the area under study, respectively. The resulting apparent P_n velocity (V'_{ij} in equation (3)) values are plotted in Fig. 3 against distance (X'_{ij}). In Fig. 3, the trend of increasing V'_{ij} with X'_{ij} is obvious, indicating the existence of the mantle P velocity gradient. We used the method described in the last section to invert for $\overline{V}(z_0)$ and c, (Eq. (7)). The results are

$$\overline{V}(z_0) = 7.93 \pm 0.17 km/s \quad , \tag{14}$$

and

$$c = 5.5 \times 10^{-4} km^{-1} \quad . \tag{15}$$

For X'_{ij} less than about 1700 km, it is clear that the condition in equation (6) is valid. The $\overline{V}(z_0)$ and c values thus estimated predict the solid line in Fig. 3, with the dashed lines representing the standard deviations. Equation (14) gives, for the uppermost mantle in Tibet, an averaged P velocity that agrees well with 7.94 km/s by Song et al. (1985). This value is, on the other hand, lower than 8.11 km/s by Jia et al. (1981) and 8.12 km/s by Chen & Molnar (1981). The difference may be caused by the relocation and correction of mantle velocity gradient, both are conducted in this study. Our value of 7.93 km/s is also lower than 8.24 km/s by Holt & Wallace (1990) and 8.29 km/s by Zhao et al. (1991), and both were obtained by using long-period body waveforms which sample deeper parts of the mantle.

Equations (14) and (15) mean that the average velocity gradient in the lithosphere beneath the Tibetan Plateau and its surrounding regions is $3.1 \times 10^{-3} s^{-1}$ for the upper 150 km of mantle, after the effect of the Earth's sphericity is corrected. Song et al. (1985) obtained a depth-dependent velocity model for the upper mantle in Tibet. We have applied a least squares fitting to their velocity

values in the upper 150 km of mantle and obtained a velocity gradient of $2.9\times10^{-3}s^{-1}$, which agrees well with our estimate. Holt & Wallace (1990) obtained a rough estimate of $2.5\times10^{-3}s^{-1}$ for the same velocity gradient, a value not significantly different from our estimate.

LATERAL VARIATIONS IN P_n VELOCITIES AND CRUSTAL THICKNESS

The c value in equation (15) and a'_i, b'_j terms obtained were used to estimate V_{ij}^0 values (equation (5)), which were then used in the back-projection tomography to solve for s_k (equation (10)). We divided the area in and around Tibet covered by the ray paths in Fig. 2 into 984 cells of a size of 1.5° by 1.5°. Convergence in the back-projection calculation takes place after 20 iterations. The resulting 2D P velocity image is shown in Fig. 4.

To estimate the lateral variations in the crustal thickness using the inverse method described earlier, we divided the area under study into 28 sub-regions. We set a linear least-squares problem to solve for τ_l, which are then used to estimate crustal thicknesses within the sub-regions (Table 3 and Fig. 5).

The overall pattern of the 2D P velocity image in Fig. 4 is characterized by a low velocity (down to about 7.78-7.83 km/s) region in north central Tibet, and high velocity regions in the north-eastern and western flanks of Tibet. This correlates well with the regional variations in S-P travel times reported by Molnar & Chen (1984), Pettersen & Doornbos (1987) and Molnar (1990). In Fig. 5, many of the areas inside Tibet have great (> 70 km) crustal thicknesses. Crustal thickness generally decreases toward and beyond the boundaries of the plateau; the rate of decrease appears to be lower toward the eastern boundary than toward the other boundaries. Next, we compare regional values of our P velocity image and crustal thicknesses with the previous localized studies.

For western Tibet (west to 80°E), including Hindu Kush and Pamir, we obtained P wave velocities in the uppermost mantle of between about 8.03 and 8.11 km/sec (Figure 4), and the crustal thicknesses of between about 65 and 70 km (Figure 5). These results agree well with previous values obtained within the same area using various methods (Beloussov et al., 1980; Kaila, 1981; Holt & Wallace, 1990; Zhao & Helmberger, 1993). Beneath station KSH we obtained a crustal thickness of 44 km (Group 11 of Table 3; Figure 5). This station is located near the western margin of the Tarim Basin, where the crustal thickness changes rapidly (Feng, 1985; Zhao et al., 1991). This probably explains why Feng et al. (1981) and Feng (1985) suggested a greater crustal thickness of 50 km inside the Basin.

Along the foothills of the Himalaya (the southern boundary of the Tibetan Plateau), we obtained P_n velocities of 7.85 - 8.01 km/sec. These values agree well with the results from travel time studies by Kaila at al. (1968), Verma (1974) and that from P_{nl} waveform inversion by Holt & Wallace (1990). Our value is also consistent with the values obtained for the Indian subcontinent from deep seismic sounding (DSS) studies (eg., Kaila, 1986; Kaila et al., 1990a, 1990b). Beyond the southern boundary of Tibet, we obtained crustal thicknesses of 34 ± 4 km and 38 ± 4km for two western locations, and 35 ± 3 km and 29 ± 3 km for two central locations (Fig. 5). The latter values agree well with the estimated thickness by Kaila et al. (1968) and Verma (1974). Our estimates of crustal thickness also agree well with those by Holt & Wallace (1990) with an exception near the western end of the southern boundary, where the thickness by Holt & Wallace (1990) is about 8 km greater than ours.

In central Tibet (80°-90°E), we obtained low P_n velocities (7.79 to 7.95 km/s). Holt & Wallace (1990, Fig. 9b) suggested a much higher velocity (8.24 km/s). Their high velocity may result from the effect of velocity gradient in the

mantle. Our estimated crustal thicknesses range between 72 and 80 km, consistent with 71.9 km by Holt & Wallace (1990).

In the Lhasa block, there have been three DSS profiles, i.e., 1 (28.8°N, 85.5°E) - (28.6 °N, 90.3°E), 2 (32.3°N, 91.4°E) - (27.4°N, 89.2°E), and 3 (32.0°N, 89.1°E) - (32.0°N, 94.5°E), during the Sino-Franco Joint Project. For this block, we obtained P_n velocities of 7.88 to 8.00 km/s, and crustal thicknesses of 75 km in the north, and 50 km in the south. The crustal thickness from interpreting the DSS profiles were 70-77 km along profile 1 (eg., Hirn et al., 1984a; Teng et al., 1983b, 1985b; Xiong et al., 1985); 75 to 40 km from north to south along profile 2 (eg., Hirn et al., 1984b, 1984c; Hirn & Sapin, 1984; Institute of Geophysics, 1981; Teng et al., 1983a); and 70 km along profile 3 (Sapin et al., 1985; Teng et al., 1985b). These agree well with our estimates. Along profile 1, Teng et al. (1983b, 1985a) suggested P_n velocities of 8.1-8.2 km/sec, whereas Hirn et al. (1984a) suggested a much higher value of 8.7 km/s. Along profile 2, Teng et a'. (1981; 1983a) and Institute of Geophysics (1981) estimated P_n velocities of 7.95-8.4 km/s. These wide ranges in the estimates of P_n velocities maybe due to many factors, including the ambiguity of P_n arrivals, the dipping Moho, error in the crustal velocity structures used, and the narrow distance range involved.

In southeastern Tibet (south to 35°N and east to 95°E), including the Yunnan and Sichuan provinces, we obtained P_n velocities that increase from 7.81 km/s in the southeast to 7.95 km/s in the northwest. The crustal thickness estimated for the interior of this area is subject to fairly large uncertainties (40 $\pm$ 17 km; see Fig. 5). This is because only 7 arrivals are available for the estimate (group 21 in Table 3). The real averaged crustal thinkness near that location may be well above 60 km. Our estimated crustal thickness is 40 $\pm$ 5 km beneath station KMI; and is 51 $\pm$ 6 km beneath stations CDN and CD2 (Fig. 5). These results agree with, within the uncertainties, the P_n velocities and crustal

thicknesses by Holt & Wallace (1990). Previous studies have suggested a changing crustal thickness from 37 to 70 km, as well as changing P_n velocity from 7.75 to 8.10 km/sec (eg., Feng, 1985; Hu et al., 1986; Zhu et al., 1986, Xiong et al., 1986; Zhao & Zhang, 1987; Yin et al., 1988; Kan & Lin, 1988) for this area.

To summarize the above comparisons, the distributions of both P_n velocity and crustal thickness in Figs 4 and 5 generally agree with, within uncertainties, previous results wherever available. It is interesting that the low ve s in north central Tibet coincide not only with the S-P residual lows previously obtained, but also with the locations where young, Cenozoic volcanic rocks have been observed (Burke et al., 1974; Kidd, 1975; Deng, 1978; Sengor & Kidd, 1979; Molnar et al., 1987). These support the hypothesis by Molnar (1988, 1990) that convective upwelling may be occurring in north central Tibet, and downwelling may be occurring in surrounding regions.

ANALYSIS OF RESOLUTION AND ERROR

In this section we quantitatively assess the quality of the 2D P-velocity image obtained in this study. We also analyze, in a less rigorous manner, the uncertainty of the crustal thicknesses reported in the earlier section.

Resolution of the P velocity image

In computerized tomography, the spatial resolution at a given cell can be approximated by the point spreading function (p.s.f.) calculated for the cell (eg., Humphreys & Clayton, 1988; Xie & Mitchell, 1990). We calculated the p.s.f for many cells in Tibet. Figs 6a, 6b and 6c show p.s.f. at three representative cells located in western, central, and eastern Tibet, respectively. As illustrated by these examples, the spreading of the p.s.f (and therefore the resolution) is generally within about 10°. At some locations where the ray coverage is relatively

denser, the p.s.f approaches to less than 6° (Fig. 6b).

Effects of random errors on P velocity image

The random errors in event locations and origin times, and in the P_n travel time readings can cause random errors in the 2D P velocity image. The events used in this study have been relocated, the errors in origin times are given in Table 1. Since there is a direct relationship between the errors in event origin times and the errors in event locations, the errors listed in Table 1 actually represent combined errors in all of the event parameters, including both event origin times and in event locations (Zhao & Helmberger, 1991). There are also probable errors in the ISC picks of the P_n arrival times, for which we estimated a maximum amplitude of 1 s. The estimated maximum amplitude of the probable errors in our own picks is 0.5 s. We think these are good estimates since the events are fairly large ($m_b > 5.5$). To estimate the random errors in the P-velocity image caused by these errors and uncertainties, we used the estimated amplitudes for the latter and a pseudo-random sign generator (Xie & Mitchell, 1990) to generate synthetic errors in travel time measurements. For details and advantages of using this random error generator, the reader is referred to Xie & Mitchell (1990).

Figure 7 shows the resulting estimates of the random errors. For areas inside Tibet, the estimated random errors are less than about 0.02 km/s. The errors increase toward the boundaries of Tibet because of poorer ray coverages, but the values of errors there are still quite small (less than 0.05 km/s), with two exceptional larger values in the northwest and southwest corner. We note, however, that the estimated random errors might be smaller than the "modelisation errors" including those mentioned before, and those caused by the probable anisotropy.

Sensitivity of 2D P velocity image to mantle velocity gradient

To see how sensitive the 2D P-velocity image in Fig. 4 is to the correction of mantle velocity gradient, we conducted back-projection inversion using apparent P_n velocities (V'_{ij} in equation (3)) without correcting for that gradient, i. e., we replaced V_{ij}^0 in equation (10) by V'_{ij} in the sensativity test. The resulting P-velocity image is plotted in Fig. 8. In this figure, the main features of the lateral variations in P-velocity image is roughly the same as that from inversion with the correction for the gradient (Fig. 4). However the average velocity in Fig. 8 is higher (8.04 $\pm$ 0.18 km/s). This velocity is close to those obtained by Jia et al. (1981) and by Chen & Molnar (1981), but lower than those by Holt & Wallace (1990) and that of 8.29 km/s by Zhao et al. (1991) who used long-period waves. From Figures 4 and 8, corrections of the mantle velocity gradient do not greatly affect the patterns of lateral variations in the tomographic images of P_n velocity, but affect significantly the average values of the images.

The upper mantle velocity gradient may have lateral variations, which can not be resolved from the current data set. Based on P wave travel time tomography for volcanic regions, Zhao *et al.* (1992) suggested that an upwelling may have a higher velocity gradient by about $1.0\times10^{-3}s^{-1}$ than the surrounding regions. If this is true for north central Tibet, the velocities beneath the region would be even lower than in Fig. 4.

Effects of vertical travel times at sources and receivers

As described earlier, we used model TIP and the laterally varying velocity models by Holt & Wallace (1990) to obtain a'_i and b'_j, the estimates of vertical travel times from sources and stations to Moho. These estimates were then used to estimate apparent P_n velocities, V'_{ij}, which in turn are used in the back-projection inversion. To see the effect of these a'_i and b'_j values on the final P

velocity image, we conducted a test of inversion in which we estimated d'_i and b'_j using model TIP only, which results in a constant value of 6.9 s for vertical travel times from surface to Moho. The mantle velocity gradient is not corrected in this testing inversion, which results in the P velocity image plotted in Fig. 9.

The average velocity of 8.19 ± 0.17 km/sec in Fig. 9 is even higher than that in Fig. 8. The main feature of a slower velocity region in northern central Tibet in Figs 4 and 8 seems to be preserved in Fig. 9, but the velocities near the boundary of Tibet in Fig. 9 becomes faster. This is particularly pronounced for cells near the western end and the middle of the southern boundary. This phenomenon can be explained by a thiner crust near the boundaries of Tibet, where the crustal thicknesses can be as small as 30 to 35 km. Model TIP predicted a universal 70 km-thick crust, which is most improper near the boundaries and lead to over-estimation of mantle velocities there. Nevertheless, the effects of ignoring the mantle velocity gradient and the lateral variations in vertical station-to-Moho travel times have not significantly altered the main pattern of lateral variations in P velocity image, and the average value of the P velocity image seems to be affected much more profoundly.

Effect of event relocation on P velocity image

In this study, event origin times and locations are obtained by the relocation procedure of Zhao & Helmberger (1991). Previous P_n studies used event parameters and P_n arrival times directly form the ISC bulletins. This has been the case for both P_n tomography (eg., Hearn et al., 1991) and for the P_n studies in and around Tibet (Chen & Molnar, 1981; Barazangi & Ni, 1982; Ni & Barazangi, 1983). Zhao and Helmberger (1991) found that the locations by ISC lead to an over-estimation of about 1.5% for P_n velocity in Tibet. Holt & Wallace (1990) also found that ISC locations of Tibetan events were systematically too deep, thus

leading to higher velocity estimates. To test the effects of not conducting event relocation, we conducted the back-projection inversion using the parameters by ISC bulletins, with corrections of a'_i, b'_j calculated using the model TIP, and without the corrections of mantle velocity gradient. The resulting P velocity image is plotted in Fig. 10, where the average velocity is 8.28 $\pm$ 0.19 km/s, which is similar to 8.42 km/s suggested by Barazangi & Ni (1982) and by Ni & Barazangi (1983). The main pattern of a slower north central Tibet is no longer clear in Fig. 10, and many of the faster velocities in the flanks of Tibet in Figs 4, 8 and 9 are now outside Tibet. Fig. 10 gives one a misconception that nearly all of Tibet forms a large low-velocity region. This test therefore indicates that it is extremely important to relocate the events in a P_n tomography study, at least for an area like Tibet.

Errors in the crustal thickness estimates

The estimates of the crustal thickness plotted in Fig. 5 are obtained under the assumption that the remnant travel-time residual, after the back-projection, is dominantly caused by δa_i and δb_j in equations (8) and (9), which reflect the small-scale variations in crustal thickness near the source and stations. In making such an assumption, we have ignored the probable effects on the remnant residuals, systematically caused in each of the 28 sub-region, by (i) origin time errors, (ii) erroneous P_n arrival readings, and (iii) the deviation of the real Moho interface from the gridded, smoothly varying surface. These assumptions cannot be perfectly valid. However, the fact that high-level structural variations have been known to exist in Tibet (eg., Hirn & Sapin, 1984) suggests that our assumptions should be, to the first order, valid and that the crustal thickness thus obtained should serve as first-order approximations.

Another practical imperfection in the result of of our inversion for the crustal thicknesses is that the result may not be reliable for groups with a small number of picks (under "N" in Table 3). For one point in Fig. 5 (near 40°N, 95°E), the crustal thickness is estimated to be -23 ± 17 km, resulting from only 7 P_n travel-time residuals. We have found that the corresponding inverse matrix is singular. We think that the crustal thicknesses inferred from other groups with less than 10 arrivals (Table 3) may not be reliable.

DISCUSSION AND CONCLUSIONS

353 P_n travel times from 44 Tibetan earthquakes (Table 1) and at 46 seismic stations (Table 2) have been collected to study lateral variations in compressional velocity in the uppermost mantle underneath the Tibetan plateau. The inverse method and procedures of this study differ from those in previous P_n tomography studies in that in the current study we applied, to the travel time measurements, corrections to several important biases, such as those caused by (i) event mislocation by ISC, (ii) mantle velocity gradient and (iii) large-scale variations in crustal thicknesses.

We used a back-projection algorithm to obtain a 2D P velocity image for the uppermost mantle. We also inverted for, to the first order approximation, the crustal thicknesses in 28 sub-regions in and around Tibet.

The main results of the inversion can be summarized in the following paragraphs:

(1) The average P velocity value for the uppermost mantle in Tibet is 7.93 ± 0.17 km/s.

(2) The average P-velocity gradient in the upper 150 km of the mantle is 3.1×10^{-3} s^{-1}.

(3) The 2D P-velocity image of the region includes a low-velocity zone in north central Tibet, and two high-velocity zones in the western and eastern flanks of Tibet.

(4) In much of the area inside Tibet, the crustal thickness is greater than 70 km. Near and outside the boundaries of the plateau, there is a general trend of decreasing crustal thickness, and the rate of decrease appears to be lower toward the eastern boundary than toward the other boundaries.

Comparison of our 2D P-velocity image and estimates of crustal thicknesses with those obtained in previous localized studies shows general agreement within the uncertainties. A few exceptions can be explained by various complications in P_n propagation, such as the effects of mantle velocity gradient, which has not been taken in to account in most previous studies.

We conducted rigorous analyses of the resolution and random error in the 2D P velocity image. The spatial resolution of that image is estimated to be generally within 10°, and often within 6° where the ray coverage is dense. The random error in that image is estimated to be generally within about 0.02 km/s for locations inside Tibet. However, the systematic, "modelisation" errors might be greater. Our estimates of the crustal thicknesses are reliable only to the first-order because of the assumptions used, and the often limited number of slowness residuals available in a sub-region.

Another important finding of this study is that event relocation (correction to bias (i) mentioned above) plays a very important role in reliably retrieving the detailed lateral variations in 2D P velocity image. Corrections to biases (ii) and (iii) mentioned above, on the other hand, seem to have a greater effect on the average (DC level) of the velocity image; the average P velocity is over-estimated without these corrections.

The low-velocity region in north central Tibet found in this study coincides with the locations of low S-P travel time residuals found in localized studies by Molnar and Chen (1984), Pettersen and Doornbos (1987) and Molnar (1990). It also overlaps with the area where Neogene or younger volcanic rocks have been found (Burke et al., 1974; Kidd, 1975; Deng, 1978; Sengor & Kidd, 1979; Molnar et al., 1987). These support the hypothesis by Molnar (1988, 1990) that a convective upwelling may be occurring in north central Tibet, and downwelling occurring in surrounding regions.

REFERENCES

Barazangi, M. & Ni, J., 1982. Velocities and propagation characteristics of *Pn* and *Sn* beneath the Himalayan arc and Tibetan plateau: possible evidence for underthrusting of Indian continental lithosphere beneath Tibet, *Geology*, **10**, 179-185.

Beloussov, V. V., Belyaevsky, N. A., Borisov, A. A., Volvovsky, B. S., Volkovsky, I. S., Resvoy, D. P., Tal-Virsky, B. B., Khamrabaev, I. Kh., Kaila, K. L., Narain, H., Marussi, A. & Finetti, J., 1980. Structure of the lithosphere along the deep seismic sounding profile: Tien Shan - Pamirs - Karakoram - Himalayas, *Tectonophysics*, **70**, 193-221.

Bourjot, L., & Romanowicz, B., 1992. Crust and upper mantle tomography in Tibet using surface waves, *Geophys. Res. Let.*, **19**, 881-884.

Burke, K. C., Dewey, J. F. & Kidd, W. S. F., 1974. The Tibetan Plateau: Its significance for tectonics and petrology, *Geol. Soc. Am. Abstr. Programs*, **6**, 1027-1028.

Chen, Wang-Ping & Molnar, P., 1981. Constraints on the seismic wave velocity structure beneath the Tibetan Plateau and their tectonic implications, *J. Geophys. Res.*, **86**, 5937-5962.

Deng, W. M., 1978. Preliminary study on the petrology and petrochemistry of the Quaternary volcanic rocks, northern Tibetan Autonomous Region, *Acta Geol. Sin.*, **2**, 148-162 (in Chinese, English Abstract).

Feng, R, 1985. Crustal thickness and densities in the upper mantle beneath China - The results of three dimensional gravity inversion, *Acta Seism. Sin.* , **7**, 143-157 (in Chinese, English abstract and figure captions).

Feng, R., Zhu, J. S., Ding, Y. Y., Chen, G. Y., He, Z. Q., Yang, S. B., Zhou, H. N. & Sun, K. Z., 1981. Crustal structure in China from surface waves, *Acta Se-*

ism. Sin., **3**, 335-350 (in Chinese, English abstract and figure captions).

Hearn, T., Beghoul, N. & Barazangi, M., 1991. Tomography of the Western United States from regional arrival times, *Geophys. J. Res.*, **96**, 16369-16381.

Helmberger, D. V., 1973. Numerical seismograms of long-period body waves from seventeen to forty degrees, *Bull. Seism. Soc. Am.*, **63**, 633-646.

Hirn, A., Jobert, G., Wittlinger, G., Xu, Z. X. & Gao, E., Y., 1984a. Main features of the upper lithosphere in the unit between the high Himalayas and the Yarlung Zangbo Jiang suture, *Annales Geophysicae*, **2**, 113-118.

Hirn, A., Lepine, J. - C., Jobert, G., Sapin, M., Wittlinger, G., Xu, Z. X., Gao, E. Y., Wang, X. J., Teng, J. W., Xiong, S. B., Pandey, M. R. & Tater, J. M., 1984b. Crustal structure and variability of the Himalayan border of Tibet, *Nature*, **307**, 23-25.

Hirn, A., Nercessian, A., Sapin, M., Jobert, G., Xu. Z. X., Gao, E. Y., Lu, D. Y. & Teng, J. W., 1984c. Lhasa block and bordering sutures - a continuation of a 500 - km Moho traverse through Tibet, *Nature*, 25-27.

Hirn, A. & Sapin, M., 1984. The Himalayan zone of crustal interaction: suggestions form explosion seismology, *Annales Geophysicae*, **2**, 123-130.

Holt, W. E. & Wallace, T. C., 1990. Crustal Thickness and upper mantle velocities in the Tibetan Plateau region from the inversion of regional P_{nl} waveforms: Evidence for a thick upper mantle lid beneath southern Tibet, *J. Geophys. Res.* **95**, 12499-12525.

Hu, H. X., Lu, H. X., Wang, C. Y., He, Z. Q., Zhu, L. B., Yan, Q. Z., Fan, Y. X., Zhang, G. Q. & Deng Y. E., 1986. Explosion investigation of the crustal structure in western Yunnan Province, *Acta Geophys. Sin.*, **29**, 133-144 (in Chinese, English abstract).

Humphreys, E. & Clayton, R. W., 1989. Adaptation of back projection tomography to seismic travel time problems, *J. Geohys. Res.*, **93**, 1073-1086.

Institute of Geophysics, Chinese Academy of Sciences, 1981. Explosion seismic study for velocity distribution and structure of the crust and upper mantle from Damxung to Yadong of Xizang (Tibet) Plateau, *Acta Geophys. Sin.*, **24**, 155-170 (in Chinese, English abstract).

Jia, S. J., Chao, X. F., 1981. P wave travel times and upper mantle velocity structure beneath Qinghai-Xizang Plateau, *N. West Seism. J.*, **3**, 27-34.

Kaila, K. L., 1981. Structure and seismotectonics of the Himalaya - Pamir Hindu Kush region and the Indian plate boundary, in Gupta, H. K. & Delany, F. M. ed. *Zagros·HinduKush·HimalayaGeodynamicEvolution*, American Geophysical Union, 272-293.

Kaila, K. L., 1986. Tectonic framework of Narmada - Son lineament - a continental rift system in central India from deep seismic soundings, in Barazangi, M. & Brown L. ed. *Reflection Seismology, A Global Perspective*, American Geophysical Union, 133-150.

Kaila, K. L., Reddy, P. R. & Narin, H., 1968. Crustal structure in the Himalayan Foot hills area of north India, from P wave data of shallow earthquakes, *Bull. Seism. Soc. Am.*, **58**, 597-612.

Kaila, K. L., Murty, P. R. K., Rao, V. K. & Venkateswarlu, N., 1990a. Deep seismic sounding in the Godavari Graben and Godavari (coastal) Basin, India, *Tectonophysics*, **173**, 307-317.

Kaila, K. L., Tewari, H. C., Krishna, V. G., Dixit, M. M., Sarkar, D. & Reddy, M. S., 1990b Deep seismic sounding studies in the north Cambay and Sanchor basins, India, *Geophys. J. Int.*, **103**, 621-637.

Kan, R. J. & Lin, Z. Y., 1988. A preliminary study on the crustal and upper mantle structure in Yunnan, *Earthq. Res. in China*, **2**, 183-202.

Kidd, W. S. F., 1975. Widespread late neogene and quaternary calc-alkaline volcanism on the Tibetan Plateau, *EOS*, **56**, 453.

Molnar, P., 1988. A review of geophysical constraints on the deep structure of the Tibetan Plateau, the Himalaya and the Karakoram, and their tectonic implications, *Phil. Trans. R. Soc. Lond.*, **A326**, 33-88.

Molnar, P., 1990. S - wave residuals from earthquakes in the Tibetan region and lateral variations in the upper mantle, *Earth Planet. Sci. Lett.* , **101**, 68-77.

Molnar, P., Burchfield, B. C., Zhao, Z. Y., Liang, K. Y., Wang, S. J. & Huang M. M., 1987. Geologic evolution of Northern Tibet: Results of an expedition to Ulugh Muztagh, *Science*, **235**, 299-305.

Molnar, P. & Chen, W. P., 1984. S-P wave travel time residuals and lateral inhomogeneity in the mantle beneath Tibet and the Himalaya, *J. Geophys. Res.*, **89**, 6911-6917.

Ni, J. & Barazangi, M., 1983. High frequency seismic wave propagation beneath the Indian Shield, Himalayan arc, Tibetan Plateau and surrounding regions: High uppermost mantle velocities and efficient *Sn* propagation beneath Tibet, *Geophys. J. R. astr. Soc.*, **72**, 665-681.

Pettersen, O. & Doornbos, D. J., 1987. A comparison of source analysis methods as applied to earthquakes in Tibet, *Phys. Earth Plant. Int.*, **47**, 125-136.

Sapin, M., Wang, X. J., Hirn, A. & Xu, Z. X., 1985. A seismic sounding in the crust of the Lhasa block, Tibet, *Annales Geophysicae*, **3**, 637-646.

Sengor, A. M. C. & Kidd, W. S. F., 1979. Post-collisional tectonics of the Turkish-Iranian Plateau and a comparison with Tibet, *Tectonophysics*, **55**, 361-376.

Song, Z. H., An, C. Q., Wang, C. Y., Zhang, L. J. & Qiu Z. R., 1985. The P wave velocity of upper mantle beneath Qinghai - Tibet Plateau and North - South seismic zone, *Acta Geophys. Sin.*, **28**, Supp. I, 148-160 (in Chinese, English Abstract).

Suetsugu, D. & Nakanishi, I., 1985. Tomographic inversion and resolution for

Rayleigh wave phase velocities in the Pacific Ocean, *J. Phys. Earth*, **33**, 345-368.

Tarantola, A., 1987. *Inverse problem theory*. Elsevier, New York.

Teng, J. W., Xiong, S. P., Sun, K. Z., Yin, Z. X., Yao, H., Chen, L. F., Mu, T., Lai, M. H., Wu, M. C., Su D. Y., Wang S. Z., Huang W. J., Ou, R. S., Hao, W. C., Shao, A. M., Gao, E. Y., Wang, M. L., Lin, Z. Y. & Qu, K. X., 1981. Explosion seismological study for velocity distribution and structure of the crust and upper mantle from Damxung to Yadong of the Xizang Plateau, *Acta Geophys. Sin.*, **24**, 155-170 (in Chinese, English abstract). Also in *Geological and Ecological Studies of Qinghai - Xizang Plateau*, Science Press Beijing, 691-710.

Teng, J. W., Sun K. Z., Xiong S. B., Yin, Z. X., Yao H. & Chen, L. F., 1983a. Deep seismic reflection waves and structure of the crust form Dangxung to Yadong on the Xizang Plateau (Tibet), *Phys. Earth Plant. Int.*, **31**, 293-306.

Teng, J. W., Xiong, S. B., Yin, Z. X., Xu, Z. X., Wang, X. J., Lu, D. Y., Jobert, G. & Hirn, A., 1983b. Structure of the crust and upper mantle pattern and velocity distributional characteristics at northern region of the Himalayan mountains, *Acta Geophys. Sin.*, **26**, 525-540 (in Chinese, English Abstract).

Teng, J. W., Xiong, S. B., Yin, Z. X., Wang, X. J. & Lu, D. Y., 1985a. structure of the crust and upper mantle pattern and velocity distributional characteristics in the northern Himalayan mountain region, *J. Phys. Earth*, **33**, 157-171.

Teng, J. W., Yin, Z. X. & Xiong, S. B., 1985b. Crustal structure and velocity distribution beneath the Serlin Co - Peng Co - Naqu - Suo county region in the northern Xizang (Tibet) Plateau, *Acta Geophys. Sin.*, **28**, Supp. I, 28-42 (in Chinese, English Abstract).

Verma, G. S., 1974. Structure of the foot-hills of the Himalayas, *Pure Appl. Geo-*

phys., **112**, 18-26.

Xie, J. & Mitchell, B. J., 1990. A back-projection method for imaging large-scale lateral variations of Lg coda Q with application to continental Africa, *Geophys. J. Int.*, **100**, 161-181.

Xiong, S. B., Teng J. W. & Yin, Z. X., 1985. The thickness of the crust and undulation of discontinuity in Xizang (Tibet) Plateau, *Acta Geophys. Sin.*, **28**, Supp. I, 16-27 (in Chinese, English Abstract).

Xiong, S. B., Teng, J. W., Yin, Z. X., Lai, M. H. & Huang, Y. P., 1986. Explosion seismological study of the structure of the crust and upper mantle at southern part of the Panxi tectonic belt, *Acta Geophys. Sin.*, **29**, 235-244 (in Chinese, English Abstract).

Yin, X. H., Liu, Z. P., Wu, J. X., Wang, C. H. & Liu, T. S., 1988. The features of Bouguer gravity field and structures of crust - upper mantle in the transition zone on the eastern border of Qinghai - Xizang - Mongolian Plateau, *Seismology and Geology*, **10**, 143-150 (In Chinese, Abstract and Figure Captions in English).

Zhao, D., Hasegawa, A., & Hirouchi, S., 1992. Tomographic imaging of P and S wave velocity structure beneath northeastern Japan, *J. Geophys. Res.*, **97**, 19909-19928.

Zhao, L. S., 1993. Lateral variations in Pn velocities beneath Basin and Range province, Submitted to *J. Geophys. Res.*.

Zhao, L. S. & Helmberger, D. V., 1991. Geophysical implications from relocations of Tibetan earthquakes: Hot lithosphere, *Geophys. Res. Lett.*, **18**, 2205-2208.

Zhao, L. S. & Helmberger, D. V., 1993. Source retrieval from broadband regional seismograms; Hindu Kush region, *Phys. Earth Planet. Int.*, in press.

Zhao, L. S., Helmberger, D. V. & Harkrider, D. G., 1991. Shear-velocity structure of the crust and upper mantle beneath Tibetan and southeastern China.

Geophys. J. Int., 105, 713-730.

Zhao, Z. & Zhang R. S., 1987. Primary study of crustal and upper mantle velocity structure of Sichuan Province, *Acta Seism. Sin.*, 9, 154-166 (in Chinese, Abstract and Figure Captions in English).

Zhu, P. D., Li, Y. M., Zhang, L. M., Shu, P. Y. & Liang, S. H., 1986. On the study of the crust and upper mantle structure beneath the seismic telemetry network in south Sichuan and north Yunnan Provinces, *Acta Geophys. Sin.*, 29, 245-254 (in Chinese, English Abstract).

Table 1. Earthquakes used in this study†

Event	Date			Origin Time			Location		Depth	N‡
	Mo	Da	Yr	hr	min	sec	(°N	°E)	(km)	
1	3	16	64	1	5	13.5 ± 1.2	37.11	95.60	10	2
2	3	6	66	2	10	52.1 ± 0.8	31.50	80.53	11	4
3	3	6	66	2	15	49.8 ± 1.1	31.48	80.50	8	3
4	10	14	66	1	4	40.0 ± 1.2	36.50	87.46	8	7
5	8	15	67	9	21	-2.6 ± 0.9	31.23	93.56	8	2
6	8	30	67	4	22	01.8 ± 1.2	31.71	100.24	10	1
7	8	30	67	11	9	44.8 ± 1.4	31.73	100.28	8	1
8	3	24	71	13	54	15.2 ± 1.2	35.46	98.03	7	1
9	4	3	71	4	49	-2.2 ± 1.4	32.19	95.08	8	1
10	5	22	71	20	3	27.3 ± 1.3	32.42	92.11	8	3
11	8	30	72	15	14	05.0 ± 1.3	36.64	96.35	15	1
12	8	30	72	18	47	38.0 ± 1.2	36.71	96.46	19	2
13	2	6	73	10	37	06.1 ± 1.5	31.38	100.54	10	1
14	2	7	73	16	6	20.7 ± 1.3	31.58	100.28	8	1
15	7	14	73	4	51	16.1 ± 1.5	35.25	86.41	6	12
16	7	14	73	13	39	24.1 ± 0.7	35.30	86.51	7	10
17	11	18	77	5	20	06.7 ± 1.1	32.75	88.44	10	8
18	3	29	79	7	7	15.3 ± 1.3	32.55	97.28	10	7
19	2	22	80	3	2	42.8 ± 0.7	30.65	88.61	10	9
20	6	1	80	6	19	-5.2 ± 1.1	39.06	95.63	12	7
21	6	24	80	7	35	44.7 ± 1.2	33.02	88.46	11	10
22	7	29	80	14	58	39.4 ± 1.0	29.64	81.08	15	7
23	8	23	80	21	36	48.9 ± 1.5	33.07	75.69	14	6
24	8	23	80	21	50	-0.5 ± 2.0	32.89	75.83	13	6
25	10	7	80	9	32	03.0 ± 1.3	35.63	82.21	4	7
26	11	19	80	19	0	45.5 ± 0.9	27.47	88.80	14	8
27	1	23	81	21	13	46.5 ± 1.2	30.99	101.14	8	5
28	6	9	81	22	8	17.6 ± 1.3	34.65	91.34	10	9
29	1	23	82	17	37	25.8 ± 1.2	31.74	82.27	10	4
30	6	15	82	23	24	26.5 ± 1.2	31.91	99.92	7	11
31	2	13	83	1	40	08.2 ± 1.9	40.05	75.17	5	11
32	5	20	85	15	11	35.6 ± 0.5	35.62	87.28	8	20
33	6	20	86	17	12	43.5 ± 1.2	31.23	86.79	15	13
34	7	6	86	19	24	20.9 ± 1.2	34.55	80.15	5	22
35	8	20	86	21	23	51.2 ± 1.2	34.65	91.49	11	15
36	8	26	86	9	43	-1.2 ± 1.4	37.83	101.55	7	7
37	2	25	87	19	56	33.3 ± 0.8	38.12	91.13	15	15
38	12	22	87	0	16	38.5 ± 1.0	41.40	89.66	20	13
39	11	5	88	2	14	29.7 ± 1.1	34.34	91.79	8	21
40	4	15	89	20	34	06.9 ± 0.9	30.04	99.13	8	15
41	4	25	89	2	13	19.5 ± 0.9	30.05	99.43	8	14
42	5	3	89	5	53	-0.7 ± 0.9	30.07	99.49	9	12
43	5	3	89	15	41	30.0 ± 0.7	30.13	99.55	8	12
44	9	22	89	2	25	49.5 ± 1.0	31.61	102.52	12	7

† The event parameters are obtained by the relocation procedure of Zhao & Helmberger (1991). In particular, the latitudes and longitudes are determined using travel times, and the depths are determined by waveform modeling of *p*, *pP* and *sP* phases. For deteails, see Zhao & Helmberger (1991).

‡ N is the number of P_n arrivals available from the event.

Table 2. Stations used in this study

Name	Location (°N)	Location (°E)	δ'_j † (sec)	N ‡
AJM	26.467	74.650	4.3	3
BRCI	27.567	81.580	3.6	2
BMI	27.300	92.200	3.6	3
BHK	31.417	76.417	4.3	4
CD2	30.910	103.758	5.1	10
CDU	30.660	104.011	5.1	6
CEP	33.824	71.909	4.3	2
CHA	26.833	87.167	3.6	4
CHCP	33.658	73.260	4.3	3
CPA	32.980	71.424	4.3	2
DDI	30.317	78.051	4.3	5
DMN	27.609	85.106	3.6	10
DRP	31.744	70.203	4.3	1
GAR	39.000	70.317	6.5	11
GTA	39.400	99.800	6.0	11
GWH	26.100	91.467	3.6	5
GYA	26.459	106.664	3.5	9
INR	27.050	93.283	4.4	7
JHI	26.733	94.167	5.1	4
JMU	32.717	74.900	3.6	2
KHM	25.651	94.068	5.1	3
KHO	37.483	71.533	6.5	13
KKN	27.784	85.268	3.6	10
KKR	29.951	76.817	4.3	6
KMI	25.123	102.740	4.1	16
KOI	26.983	95.500	5.1	5
KSH	39.450	75.968	6.0	15
LAH	31.550	74.333	4.3	8
LSA	29.700	91.150	6.9	24
LZH	36.084	103.834	6.0	19
MNL	33.135	73.750	4.3	3
NDI	28.683	77.217	4.3	24
NIL	33.650	73.250	4.3	6
PKI	27.571	85.409	3.6	9
PSH	33.937	71.434	4.3	1
PTH	29.550	80.217	5.2	4
SARP	31.922	72.670	4.3	3
SBDP	32.300	70.800	4.3	1
SHL	25.567	91.883	3.6	36
SRNI	33.950	74.750	4.3	1
THW	32.794	71.743	4.3	3
TOC	26.750	94.767	5.1	5
VAR	25.300	83.017	3.6	14
WRS	34.150	71.401	4.3	5
XAN	34.034	108.917	3.6	13
YYI	26.567	94.683	5.1	2

† δ'_j is vertical travel time from Moho to station.

‡ N is number of P_n travel times used to calculate δ'_j.

Table 3. Vertical Travel Time Corrections for Sub-regions (τ_l)

Sub-region	Stations or Events	τ_l	N†
1	GAR,KHO	0.78±0.52	24
2	CPA,CEP,CHCP,DRP,JMU LAH,MNL,NIL,PSH,SBDP SRNI,SARP,THW,WRS	-0.84±0.41	41
3	AJM,BHK,DDI,KKR,NDI PTH	-0.41±0.37	46
4	BRCI,CHA,KKN,KMN,PKI VAR	-0.70±0.35	49
5	BMI,GWH,INT,JHI,KHM KOI,SHL,TOC,YYI	-0.13±0.30	70
6	GYA,KMI	-0.06±0.50	25
7	CD2,CDU	0.02±0.59	16
8	XAN	-0.36±0.66	13
9	LZH	0.80±0.54	19
10	GTA	-0.28±0.71	11
11	KSH	-1.42±0.61	15
12	ev25,ev34	0.77±0.45	29
13	ev2,ev3,ev22,ev29	0.88±0.57	18
14	ev26	-0.69±0.82	8
15	ev4,ev15,ev16,ev32	0.47±0.37	49
16	ev17,ev19,ev21,ev33	0.49±0.38	40
17	ev31	0.18±0.72	11
18	ev37	0.06±0.60	15
19	ev29,ev35,ev39	0.08±0.36	45
20	ev5,ev9,ev10	0.85±0.95	6
21	ev18	-1.17±0.89	7
22	ev6,ev7,ev13,ev14,ev27 ev30,ev40,ev41,ev42 ev43,ev44	0.08±0.30	80
23	ev1,ev8,ev11,ev12	0.28±0.98	6
24	ev20	-4.49±0.88	7
25	LSA	0.65±0.48	24
26	ev23,ev24	-0.68±0.70	12
27	ev36	0.65±0.88	7
28	ev38	0.30±0.65	13

† N is number of travel time residuals ($\delta a'_i$ or $\delta b'_j$) used to estimate τ_l.

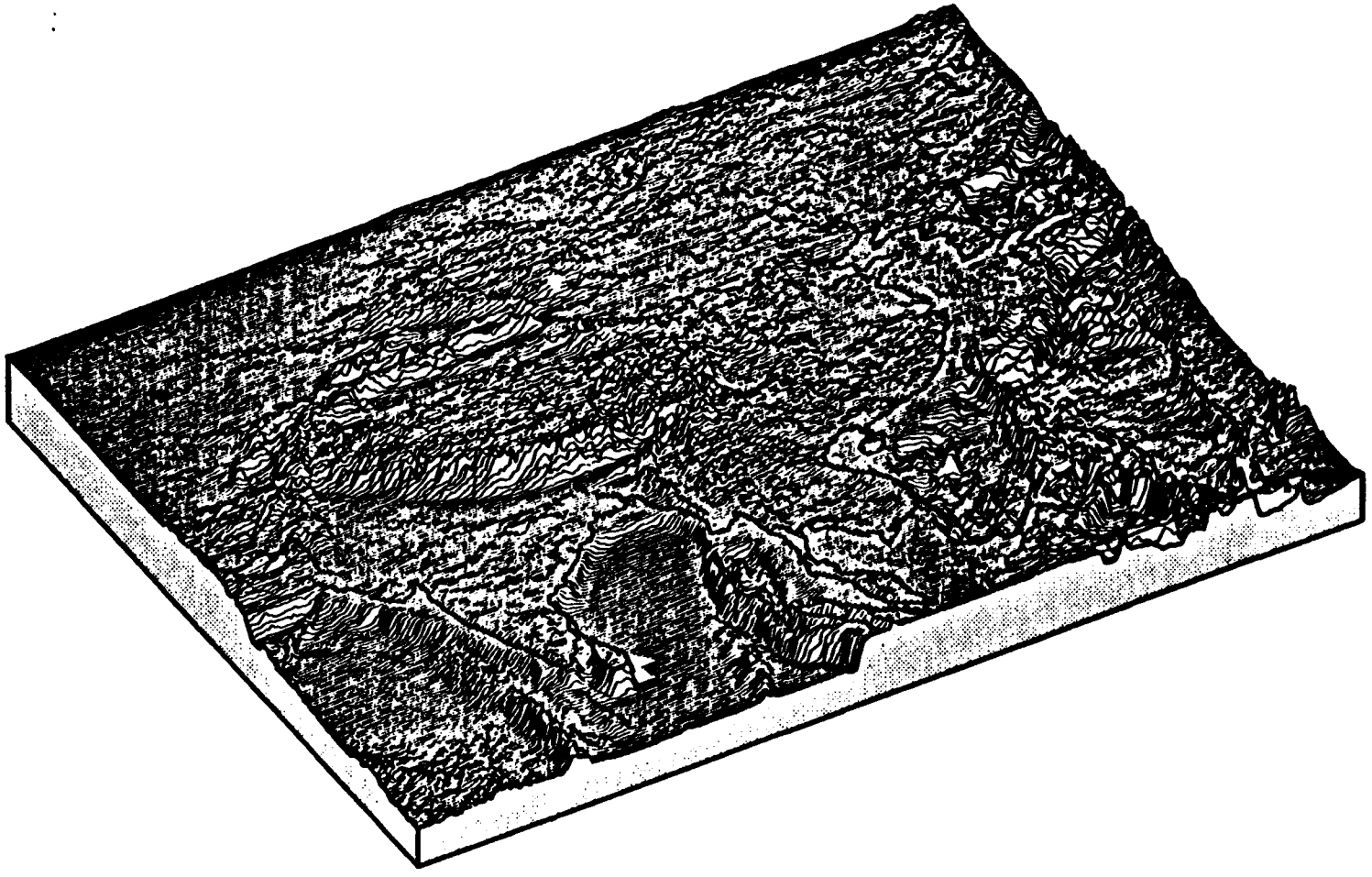

Figure 1. 3D view of the topography of the Tibetan Plateau and its surrounding regions.

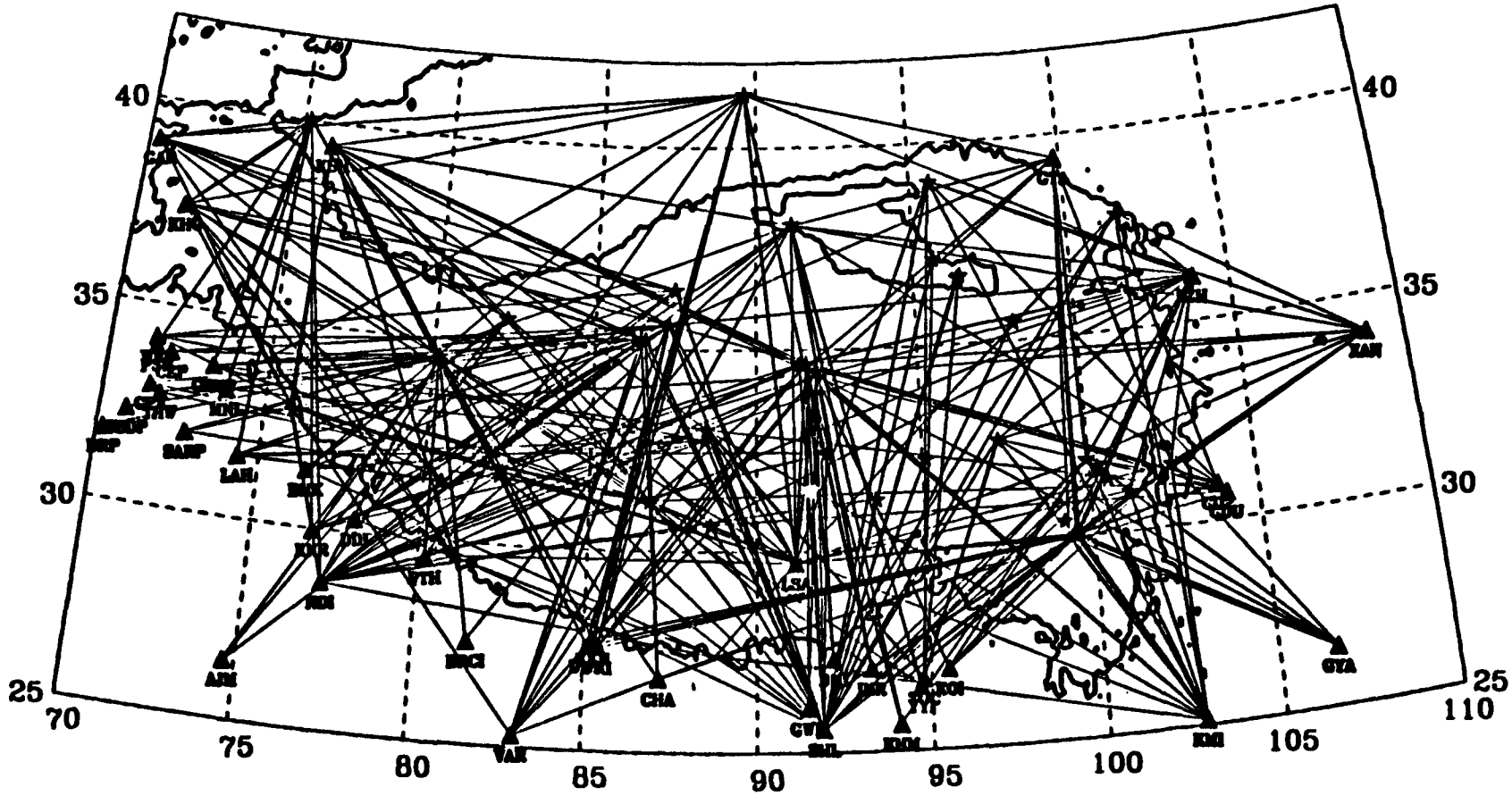

Figure 2. Ray paths. Triangles are stations. Stars are earthquakes. A heavy solid line is the contour of 3000 m altitude, which marks the boundary of the Tibetan Plateau.

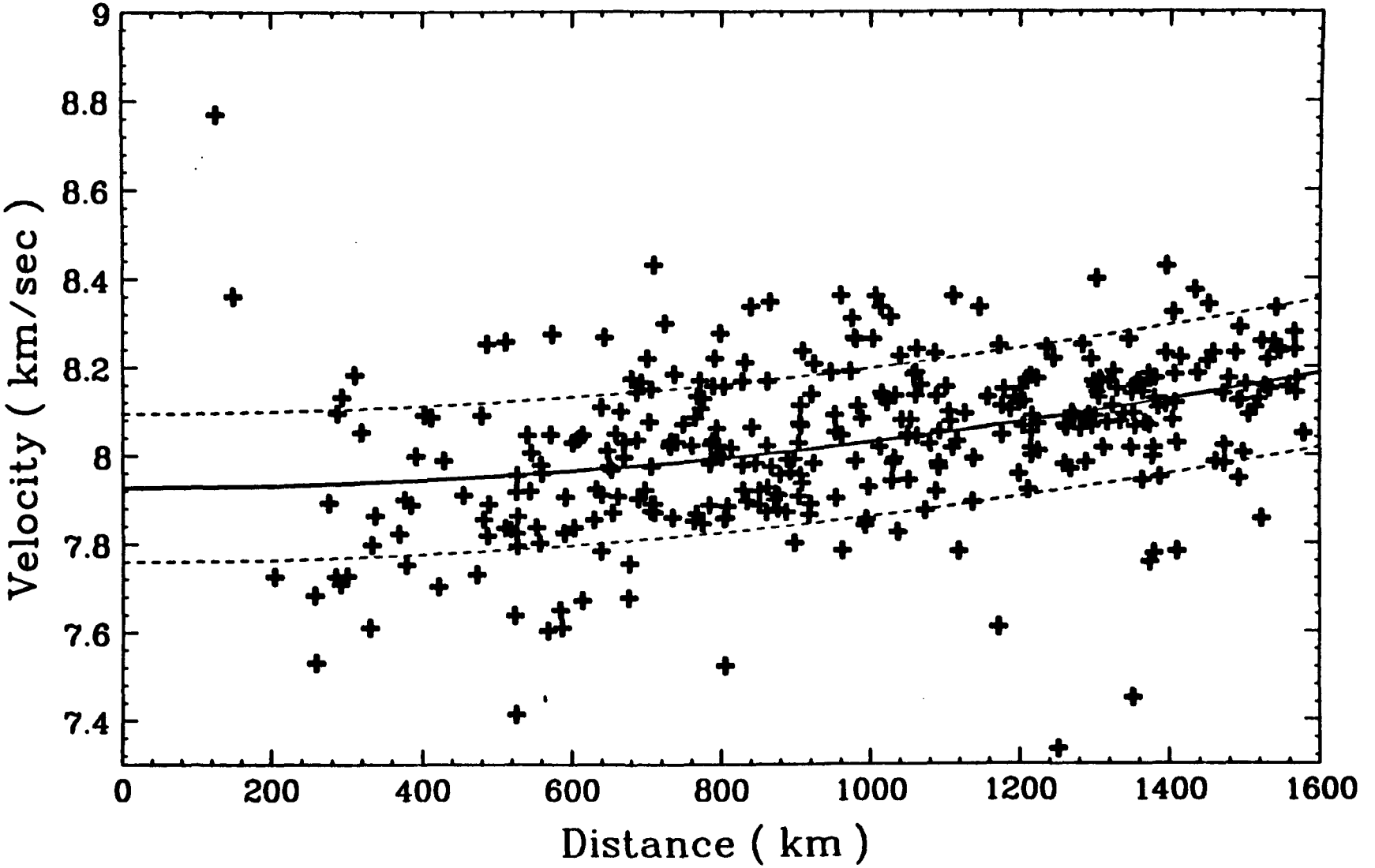

Figure 3. P_n travel time data used in this study. The abscissa is distance traveled by the head wave in the mantle. A tendency for the travel times to be dependent on the distances can be easily seen. The solid line represent the linear regression fitting of equation (5), corresponding to an average P velocity in the uppermost mantle of 7.93 km/s and an average of mantle P velocity gradient of 4.4 X 10^{-3} s^{-1} (including the Earth's sphericity). Dashed lines represent the standard errors of the fitting.

~/docum/FNN/,lnvpn/,figs/figisc.p

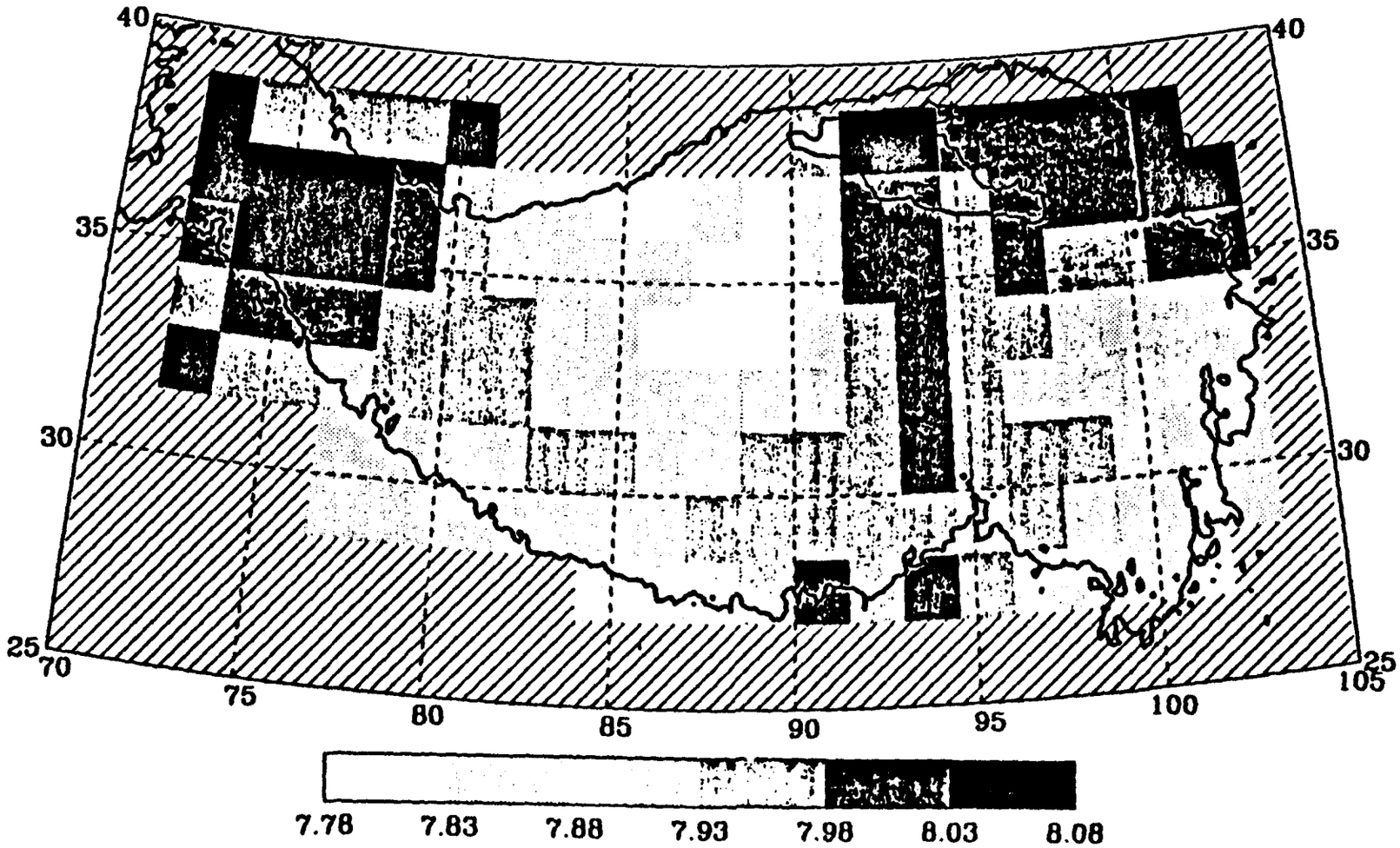

Figure 4. 2D P velocity image for the uppermost mantle underneath the Tibetan Plateau.

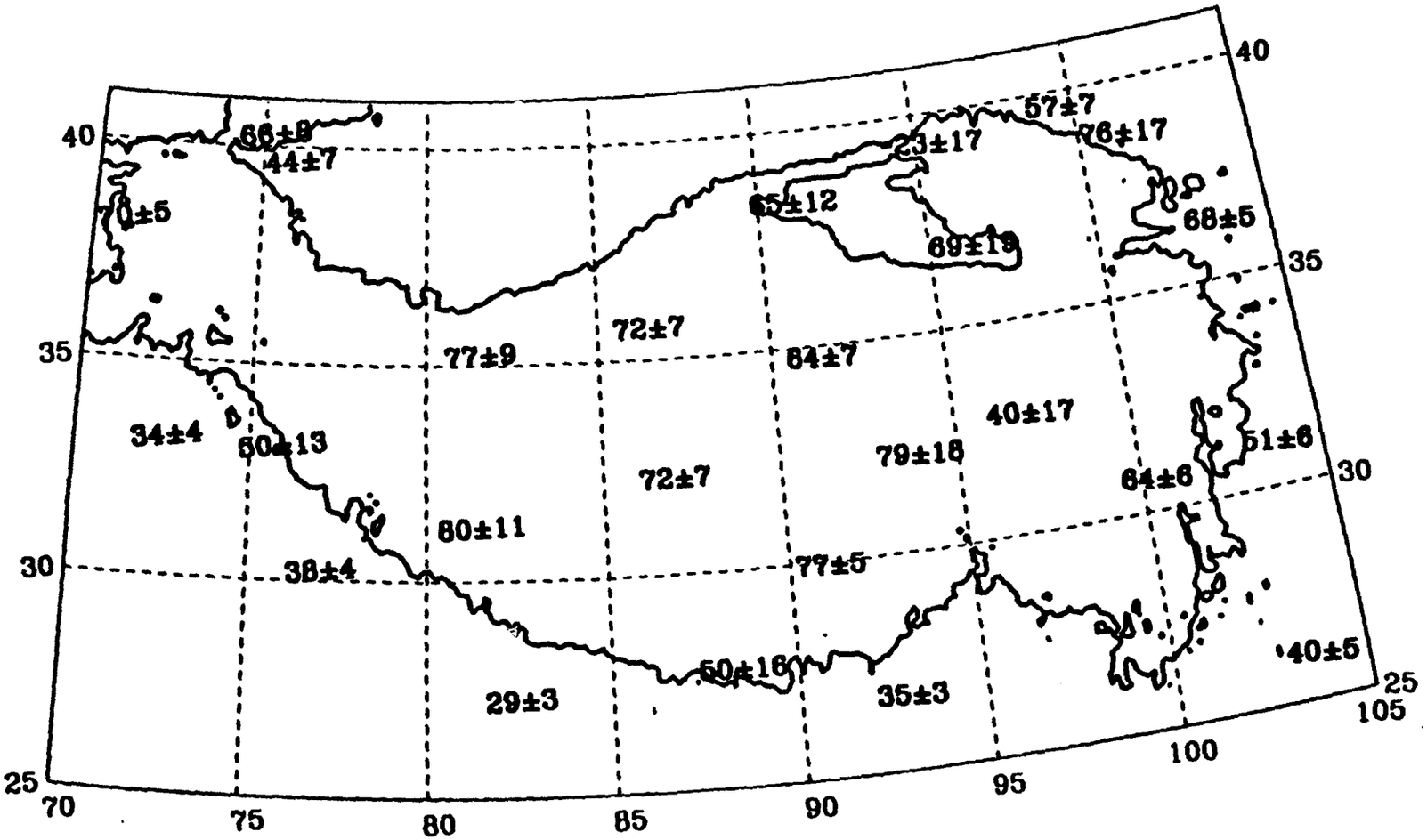

Figure 5. Crustal thicknesses of sub-regions (Table 3).

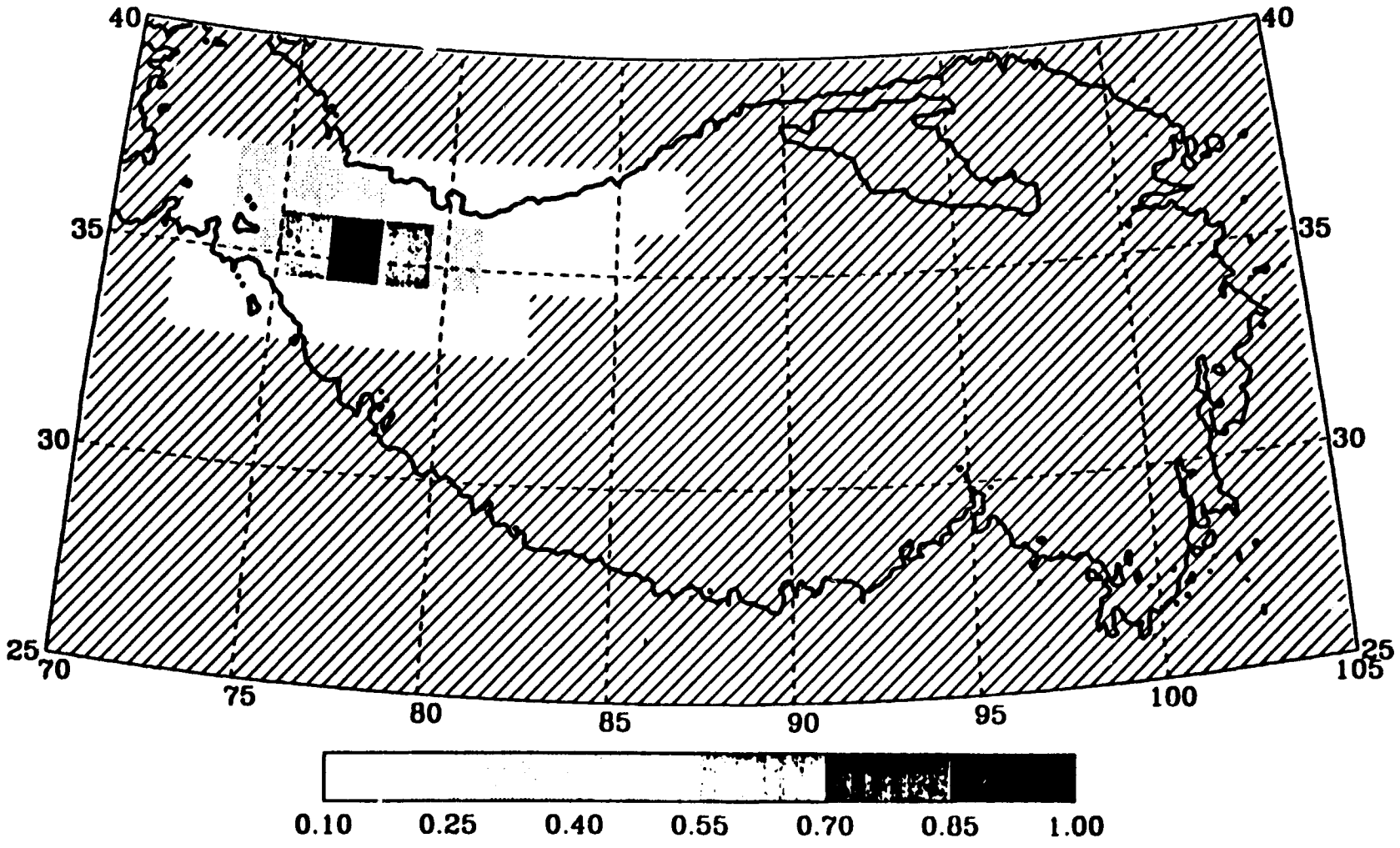

Figure 6a

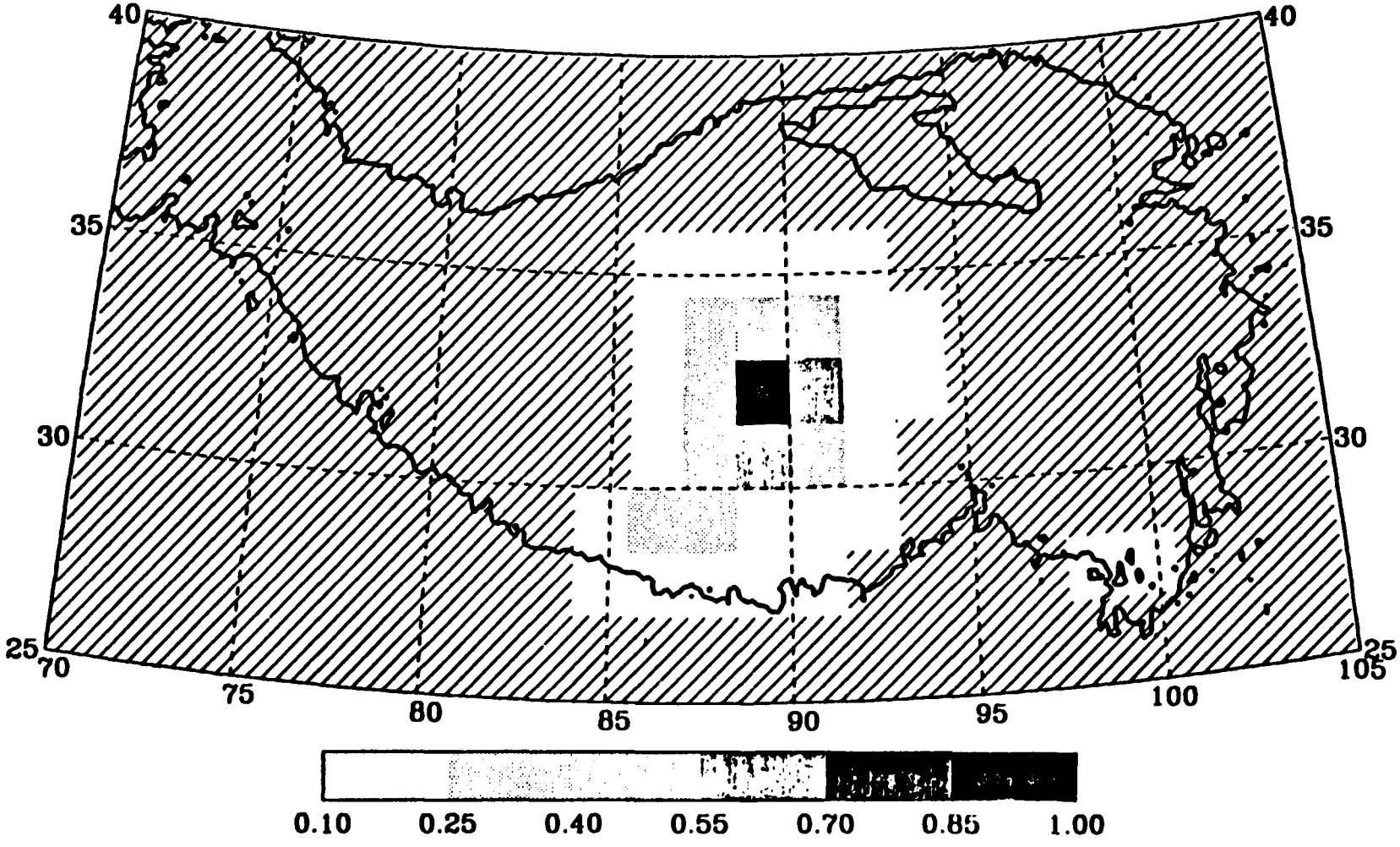

Figure 6b

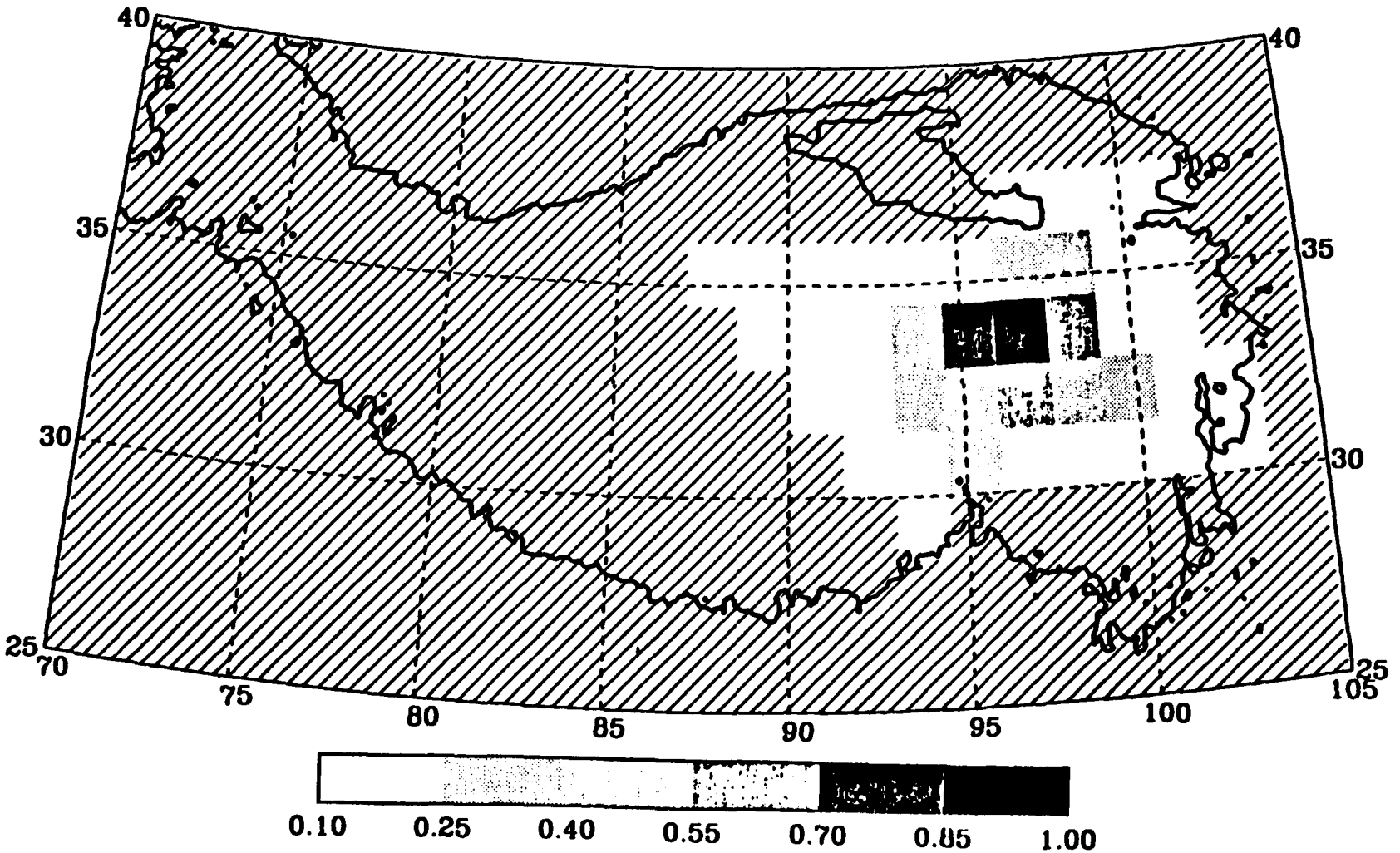

Figure 6. Point spread functions (p.s.f.). a) p.s.f. at a location in the Karakoram region of western Tibet, the p.s.f. spread out to 8°; b) near the center of Tibet, about 6°; c) at a location in eastern Tibet, about 8°.

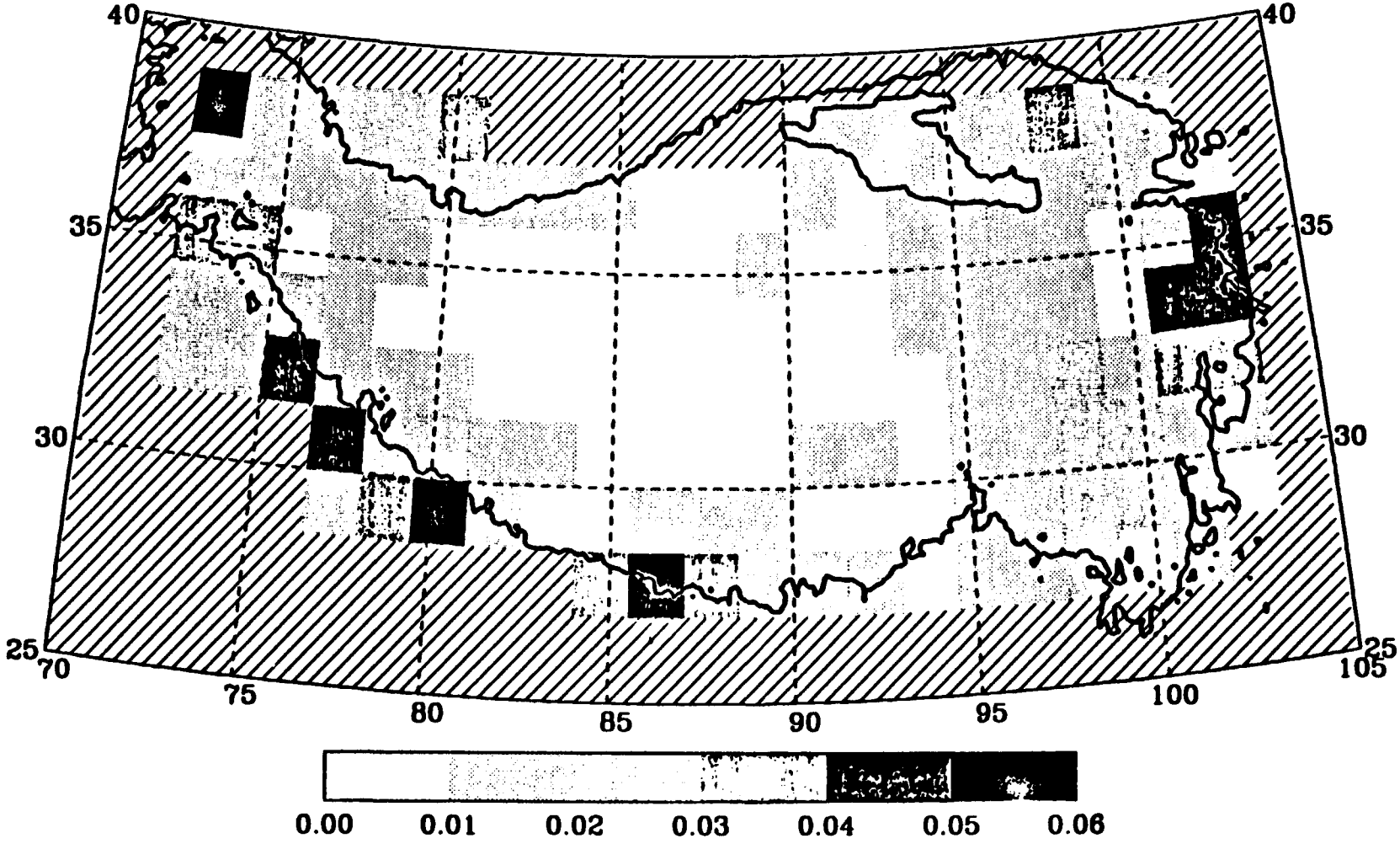

Figure 7. Map of the estimated random errors in the 2D P velocity image. Inside Tibet, the error is less than 0.02 km/sec. the error on the Tibetan boundary is generally less than 0.05 km/sec.

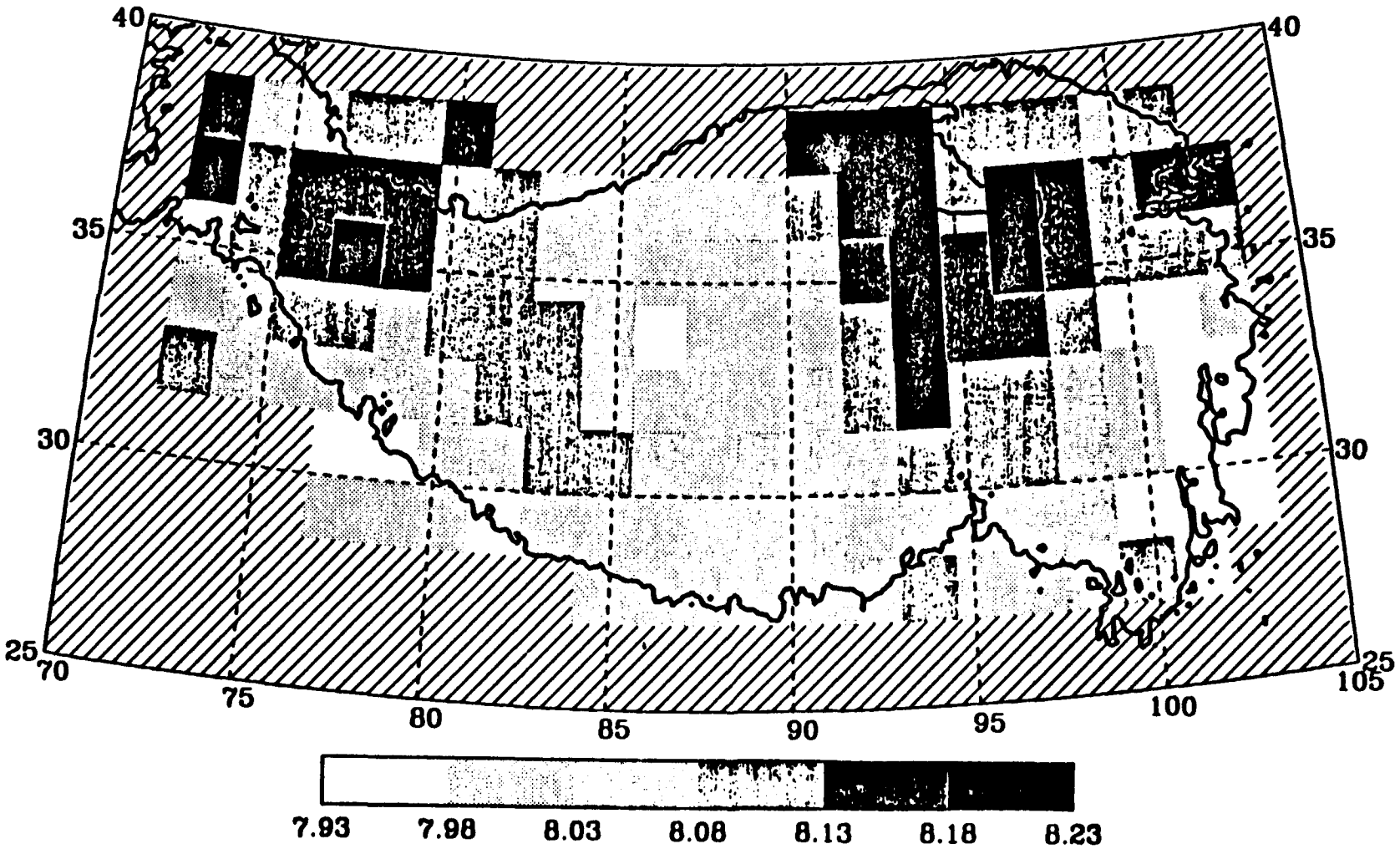

Figure 8. 2D P velocity image obtained without correcting for the mantle velocity gradient.

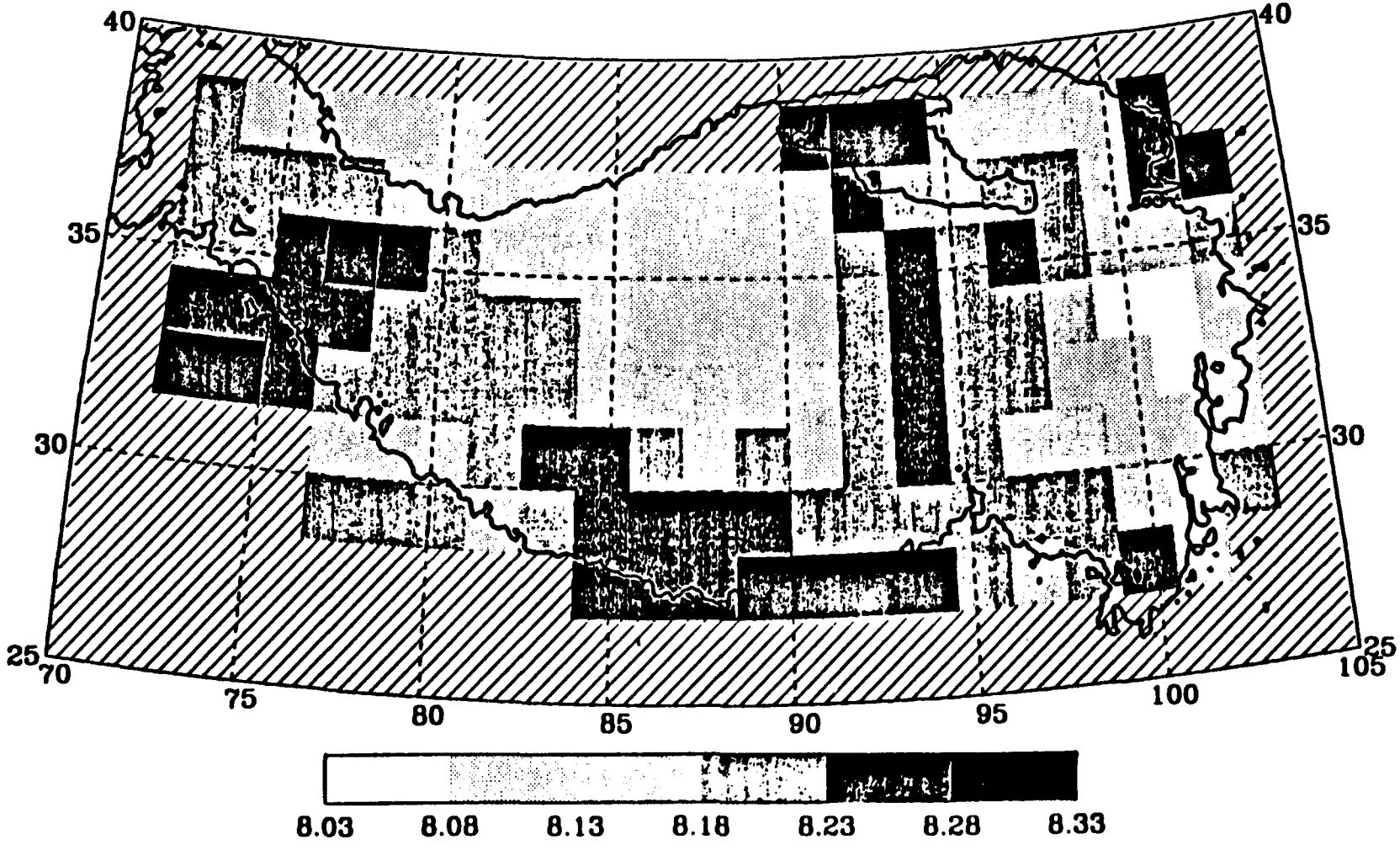

Figure 9. 2D P velocity image obtained with no corrections to the mantle velocity gradient, nor to the regionally varying vertical travel times from source/station to Moho.

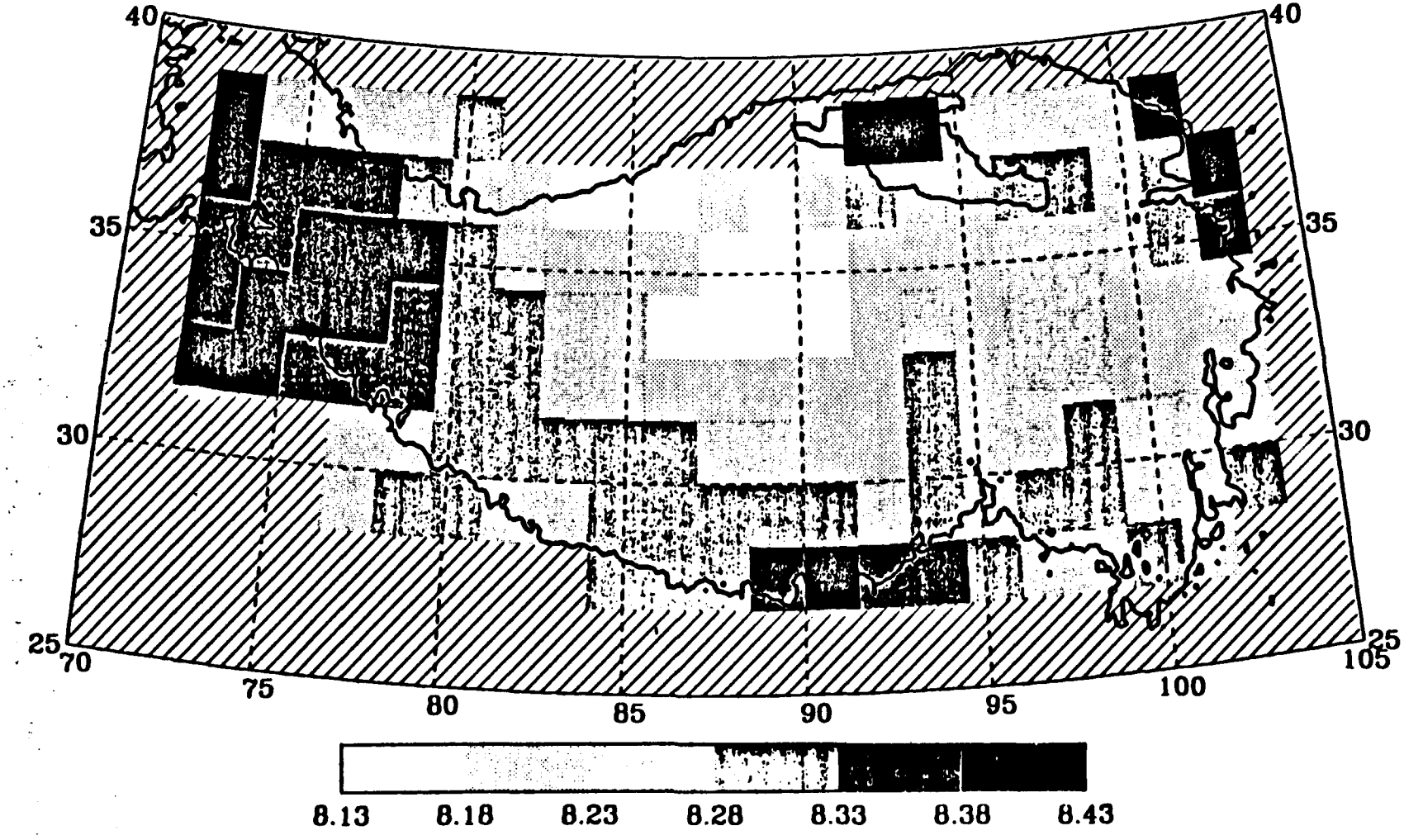

Figure 10. 2D P velocity image obtained by using all parameters, including P_n arrival time picks and the event origin times/locations, from the ISC bulletins.